Age exacerbates SARS-CoV-2-induced blood-brain barrier leakage and neuropsychiatric dysfunction

Seshadri B. Niladhuri*[1], Guliz O. Clare*[1], KaReisha F. Robinson[1], Jacob Class[2], Ali A. Almousawi[1], Troy N. Trevino[1], Felecia M. Marottoli[1], Leon M. Tai[1], Justin Richner#[2], and Sarah E. Lutz#[1&].

*Equal contribution first authors

#Equal contribution senior authors

[1] Department of Anatomy and Cell Biology, University of Illinois at Chicago, College of Medicine, Chicago, Illinois 60612, USA

[2] Department of Microbiology and Immunology, University of Illinois at Chicago, College of Medicine, Chicago, IL 60612, USA

[&]Correspondence:

Sarah E. Lutz PhD

selutz@uic.edu

ORCID 0000-0002-6388-753X

Abstract

Persistent cognitive impairment and neuropsychiatric disorders are prevalent sequelae of SARS-CoV-2-induced COVID-19 in middle-aged adults. To model age-related neurological vulnerability to COVID-19, we induced respiratory SARS-CoV-2 MA10 infections by nasal inoculation in young (2 months) and middle-aged (12 months) mice. We hypothesized that aging and SARS-CoV-2 synergistically damage the blood-brain barrier (BBB). Indeed, the combined action of aging and SARS-CoV-2 infection caused more fibrinogen leakage, T cell infiltration, and neuroinflammation in middle-aged SARS-CoV-2-infected mice than in similarly inoculated young adults. Mechanistically, SARS-CoV-2 exacerbated age-related increases in Caveolin-1 BBB transcellular permeability and loss of Wnt/β-catenin ligands, with no apparent changes in tight junction proteins. Finally, SARS-CoV-2 infection induced age-dependent neuropsychiatric abnormalities including bradykinesia and obsessive-compulsive-like behavior. These observations indicate that cerebrovascular aging, including loss of Wnt suppression of Caveolin-1, heightens vulnerability to SARS-CoV-2-induced neuroinflammation and neuropsychiatric sequalae. Our work suggests that modulation of Wnt signaling or its downstream effectors at the BBB could be potential interventional strategies for Long COVID.

Highlights

- To our knowledge, we have for the first time used a small animal model to experimentally test the impact of age on SARS-CoV-2 neuropathology.
- Aged mice were uniquely vulnerable to neuropsychiatric signs after SARS-CoV-2 infection
- Middle-age increased gliosis, cerebrovascular inflammation, BBB permeability, and T cell infiltration in SARS-CoV-2 infected mice
- BBB permeability was related to loss of Wnt7a suppression of Caveolin-1

Introduction.

Cognitive impairment ("brain fog"), executive function deficit, sensory/motor disorder, anxiety disorders, and fatigue are common cognitive and neuropsychiatric presentations of COVID-19 and Long COVID(Graham et al., 2021; Guo et al., 2022; Nalbandian et al., 2021; Taquet et al., 2021; Visvabharathy et al., 2021). We collectively refer to the neuropathologic, cognitive, and neuropsychiatric presentation of COVID-19 and Long COVID as "NeuroCOVID". The causes of NeuroCOVID are thought to include cerebrovascular inflammation(Iadecola et al., 2020; Teuwen et al., 2020). Indeed, COVID-19 patients exhibit acute cerebrovascular injury, and autopsied patient brains are riddled with a constellation of cerebrovascular abnormalities including vascular regression, basement membrane disruption, endothelial cell death, hypoxia/ischemia, BBB permeability, and leukocytic infiltration, accompanied by gliosis and loss of neurons and synapses (Nalbandian *et al.*, 2021; Schwabenland et al., 2021; Wenzel et al., 2021).

Age is an influential factor in presentation of neurological components of Long COVID. Individuals in middle and advanced age are highly susceptible to NeuroCOVID, whereas pediatric populations and adults in the age range 18-30 are more likely to recover from COVID-19 without ongoing symptoms (Guo *et al.*, 2022; Parisi et al., 2021). Even mild SARS-CoV-2 infection can precipitate ongoing neuroinflammation and neurodegeneration in susceptible age populations. Markers of endothelial inflammation and neuronal injury remain elevated in patient serum two months after mild COVID-19 in patients 36-65 years of age but are negligible in patients 18-35 (Ameres et al., 2020; Chioh et al., 2021). Rates of new onset or relapsed neuropsychiatric disorders are elevated after SARS-CoV-2 infection; this especially includes anxiety and post-traumatic stress disorder in middle-aged individuals and a dramatic increase in dementia in the advanced ages (Nalbandian *et al.*, 2021; Taquet *et al.*, 2021).

Age-related declines in cerebrovascular function and blood-brain barrier (BBB) integrity could increase susceptibility to NeuroCOVID. The BBB selectively restricts permeability of CNS blood vessels to macromolecules and immune cells from the blood. BBB damage occurs from loss of endothelial tight junctions, which normally suppress inter-cellular diffusion, and from increased rates of vesicular traffic across the endothelial cytoplasm(Knowland et al., 2014; Lutz et al., 2017; Mapunda et al., 2022). Importantly, Wnt/β-catenin signaling promotes BBB function in an age-dependent pattern. Wnt/β-catenin signaling in

cerebrovascular endothelium is required for early life induction of BBB properties (Daneman et al., 2009; Liebner et al., 2008; Stenman et al., 2008). We and others have shown that Wnt/β-catenin promotes adult BBB maintenance and repair (Lengfeld et al., 2017; Martin et al., 2022; Tran et al., 2016). SARS-CoV-2 can compromise the BBB (Krasemann et al., 2022; Reynolds and Mahajan, 2021; Zhang et al., 2021). We sought to determine, for the first time, the effect of age and infectious SARS-CoV-2 on the BBB *in vivo*. We hypothesized that age-related declines in BBB function and Wnt/β-catenin exacerbate NeuroCOVID.

To test age-dependent mechanisms of NeuroCOVID, we intranasally inoculated 2-month-old and 12-month-old C57Bl/6 mice with a strain of SARS-CoV-2 adapted for increased pathogenicity in mice by a mutation in the receptor binding domain of spike and serial passage in mice lung(Dinnon et al., 2020; Leist et al., 2020). This leads to viral replication in the lung (Dinnon *et al.*, 2020; Leist *et al.*, 2020). We find that intranasal inoculation with SARS-CoV-2 causes dissemination of viral RNA into the brain, cerebrovascular inflammation, T cell infiltration, and BBB leakage. Importantly, age increased neuroinflammation and BBB permeability, and precipitated repetitive stereotypical grooming behavior, bradykinesia, and hypokinesia. Advanced age and infection downregulated Wnt ligands known to promote BBB integrity. Thus, age strongly influences severity of BBB disruption, neuroinflammation and neuropsychiatric presentation in SARS-CoV-2 infected mice.

Materials and Methods

Mice.

C57Bl/6 mice purchased from Jackson laboratories at 8 weeks of age or at 12 months of age were housed on site in a specific pathogen free barrier suite for at least 7 days prior to initiation of experiments. Mice were transferred to the Animal BioSafety Level 3 facilities at least 2 days prior to inoculation. Mice were maintained on standard light-dark cycles with ad libitum food and water in micro-isolation cages. Cages holding 4-5 mice were randomized to either SARS-CoV-2 inoculation or vehicle (saline) inoculation groups. Mouse-adapted SARS-CoV-2 (MA10) was provided by Ralph Baric (University of North Carolina, Chapel Hill, North Carolina, USA) (Dinnon *et al.*, 2020; Leist *et al.*, 2020). SARS-CoV-2 (MA10) was propagated and titered on Vero-E6 cells (ATCC, CRL1586). Mice were anesthetized with isoflurane and challenged via intranasal inoculation with 1×10^4 foci-forming units (FFU SARS-CoV-2 MA10). Lungs or brains were isolated from mice at the indicated time post infection. Each morning mice were assessed for body condition score including body weight, coat

condition, posture, and qualitative inspection of respiratory rate and behavior. At onset of clinical signs, mice were further assessed in a battery of assays for physical and neurocognitive function before euthanasia, as described below.

Euthanasia and tissue collection

Mice were perfused with ice-cold saline under deep isoflurane anesthesia. Brains were cut in sagittal sectinos. Left brains were dissected into olfactory bulb, forebrain, brainstem, cerebellum, and spinal cord, and homogenized in either Buffer RLT for RNA isolation or in RIPA buffer for Western blotting. Right brains were immersion fixed in 4% paraformaldehyde for 48hours. Tissues were then either cryoprotected in 30% sucrose and embedded in OCT for 20 micron cryosections (Experiment 1, 2) or dehydrated and embedded in paraffin for 5 micron sections (Experiment 3). Antigen retrieval was conducted with sodium citrate buffer for 30 minutes at 95 degrees. Sections were blocked and permeabilized with 10% bovine serum albumin and 0.2% Triton-X 100 in phosphate buffered saline. Primary antibodies for immunostaining included Collagen IV (Abcam ab236640), CD3 (Abcam ab16669), Glut1 (Abcam ab40084), Fibrinogen (LS Bio LS-C150799-1), Caveolin-1 (Invitrogen PA5-17447), GFAP (Millipore c115516), and Iba1 (Abcam ab178847). Secondary antibodies were conjugated to Alexa fluorophores. Microscopy was conducted using Zeiss LSM710 or Leica DMI8 microscopes. Quantification was performed using FIJI software (NIH).

Western blotting.

Brainstem samples homogenized in RIPA buffer were quantified with BCA assay and loaded onto 12% acrylamide gels, transferred onto PVDF membranes, blocked with LiCOR Intercept Buffer, incubated with primary antibodies including Occludin (Invitrogen 71-1500), ZO-1 (Invitrogen 33-9100), Caveolin-1 (Invitrogen PA5-17447), β-actin (Abcam ab6276), incubated with LiCOR far-red conjugated secondary antibodies, and detected with LiCOR Odyssey CLX.

RNA Isolation and RT-qPCR

Tissues were homogenized in Buffer RLT. Tissues were then transferred to the BSL2 laboratory. RNA was extracted from tissue homogenate using a Zymo Research Quick-RNA 96 Kit (R1052). Viral genomes were quantified via quantitative RT-PCR with the N1 Primer/Probe Kit from Integrated DNA Technologies (IDT, 10006713). We generated cDNA using High-Capacity RNA-to-cDNA™ Kit (Applied Biosystems) following the

manufacturer's specifications. cDNA was probed with Power SYBR™ Green PCR Master Mix (Applied Biosystems) RT-qPCR. Primer sequences are: GAPDH AACTTTGGCATTGTGGAAGG, ACACATTGGGGGTAGGAACA. Cav1 GACGCGCACACCAAGGAGATT, CTGACCGGGTTGGTTTTGAT. Cldn5 GCTTCCCGGTCAAGTACTCT, CCTCCCGCCCTTAGACATAG. Ocln AGTGTGGATGACTTCAGGCA, TCATAGTGGTCAGGGTCCGT. Wnt3 CTCGGCGCTGCTTCTAATG, CTTCACACCTTCTGCTACGC. Wnt5a TCTCCTTCGCCCAGGTTGTT, CCTGTCTTCGCACCTTCTCCA. Wnt5b GCTGCTGACTGACGCCAACT, GCACTCTCTGATGCCCGTCTT. Wnt7a CGCCAAGGTCTTCGTGGATG, CGGCCTCGTTGTATTTGTCCT. Wnt7b TTTCTCGTCGCTTTGTGGATG, GCCTGACACACCGTGACACTT. Apcdd1 CCCACATTCACCATCTACGC, CACGCAGCCATTGGTATGTG. For each primer pair, a no-template control was included, and each sample was run in triplicate. Samples were tested in 384-well plates using ViiA 7 Real-Time PCR System (Applied Biosystems). The conditions were set to 50°C for 2 min, 95°C for 2 min and 40 cycles of 95°C for 15 s, and 60°C for 1 min at QuantStudio 5 Real-Time PCR System (Applied Biosystems). The experimental results indicating 90%–100% efficiency was analyzed by using the comparative Ct (ddCt) method to detect the relative expression of the target gene. RNA quantifications were normalized to glyceraldehyde-3-phosphate dehydrogenase (GAPDH) by subtracting the average Ct value with that of GAPDH for each sample. The ddCt value was calculated by subtracting the dCt value for the gene from that of the GAPDH. Finally, the relative copy number was determined as 2^{-ddCt}. The results were analyzed and plotted as the relative expression of the target by using GraphPad Prism software.

Behavioral Assays.

For novel object recognition (NOR), we first tested a catalog of 10 objects for intrinsic preference. Objects were similar in size (1-2 inches wide, 3-4 inches tall), visually interesting, without smell, and made of easily cleaned non-porous materials. Our optimal objects 25ml suspension flasks (Falcon) filled with sterile pebbles (Home Depot), rainbow-colored shotglass cups (Amazon), and bottles of glitter nail polish (Sally Hansen). All behavior tasks were conducted between 8-11AM in a dark biosafety cabinet laminar flow hood in the BSL3 facility. No habituation step was included. For familiarization on 3DPI, we placed individual mice in a dark open field containing two suspension flasks and allowed 10 minutes exploration. Behavior was filmed with an overhead mounted wide-angle webcam (Logitech C920S HD Webcam). After a 24-hour inter-session-interval, on 4DPI, mice were reintroduced into the dark open field, this time containing one suspension flask and one bottle of nail

polish, and filmed for 10 minutes. Objects and field were cleaned with ethanol and dried in between mice. The position of the novel object (left side or right side of open field) was alternated. Videos were coded and independently scored by two blinded scientists for duration of exploration of each object. Exploration was defined as face oriented toward the object in close proximity (1 inch). For the pole climb assay, the rod of a buret support stand (1/2 inch diameter, 18 inches length) mounted on a metal base was placed in a test cage. The metal base was covered with clean corn cob bedding. The latency to descend the pole and dismount onto the bedding was measured. For the composite cerebellar ataxia phenotyping, we assigned up to 3 points each for abnormal performance in the ledge test, hindlimb clasping, gait, and kyphosis, as described (Guyenet et al., 2010). Open field was conducted by filming mice for ten minutes with an overhead camera in white plastic bins 13 inches x 19 inches (Ikea) with pebbled floor in the biosafety cabinet in the dark. In the open field recordings, motility was automatically computed using Noldus EthoVision XT software. The calibration of the area and the detection for the mouse recognition were set in the software for each video. Velocity, distance traveled, time spent in the center, time spent in the edges were read for the first 10 minutes of the records as well as the relative time spent in the center for open field analysis. Relative mobility, relative immobility, mobility/immobility, time, and frequency of highly mobile states information was extracted from the software analysis and plotted by using GraphPad Prism. The data for grooming behavior of mice was manually extracted from the recorded videos. The frequency and duration of grooming was independently recorded by two blinded observers using a timer. The grooming behavior was identified by following the specific behavioral pattern as described (Kalueff et al., 2016). The number of attempts, cumulative duration, and average duration of each grooming was calculated and plotted. The statistical differences were calculated by using one-way ANOVA in GraphPad.

Results.

SARS-COV-2 induces blood-brain barrier cellular migration

To establish a mouse model with which to interrogate CNS consequences of respiratory SARS-CoV-2 infection, we inoculated C57Bl/6 mice with SARS-CoV-2 MA10 (Dinnon *et al.*, 2020; Leist *et al.*, 2020) by

intranasal route. We compared infection in mice of two ages: young adult (2 months, n=14) and middle aged (12 months, n=11). Four days post inoculation (4DPI) was designated the endpoint of the experiment.

Migration of immune cells across the blood-brain and blood-CSF barriers causes neuroinflammation (Mapunda *et al.*, 2022). We asked if neurologic consequences of SARS-CoV-2 infection are related to perivascular leukocyte infiltration across brain barriers. At 4DPI, mice were euthanized, and sagittal brain sections were prepared for histology. We conducted immunostaining for cerebrovascular basement membrane Collagen IV, together with nuclear counterstain DAPI (Fig 1A-B). In SARS-CoV-2 infected mice, we identified intense foci of cerebrovascular hypercellularity suggestive of leukocyte infiltration (Fig 1B). SARS-CoV-2 infection induced perivascular hypercellularity in both young adult and middle-aged adults, with more severe inflammation in the middle-aged group. We found an average of 25 perivascular inflammatory foci per brain section in 2-month-old infected mice, and 35 perivascular inflammatory foci per brain section in 12-month-old infected mice ($p<0.0001$, two-way ANOVA and Tukey's multiple comparisons test) (Fig 1C).

We then asked whether inflammation was restricted to parenchymal or meningeal/ventricular compartments. Barrier forming cells of the cerebrovasculature (Krasemann *et al.*, 2022; Rauti et al., 2021; Reynolds and Mahajan, 2021), meninges, and choroid plexus (Pellegrini et al., 2020; Yang et al., 2021) are potential targets of SARS-CoV-2 infection and demonstrate inflammatory changes in COVID-19 infected individuals and animal models. We therefore measured foci of inflammation in the BBB, blood-meningeal barrier, and blood-cerebral spinal fluid barrier. SARS-CoV-2 infection caused a two- to three-fold increase in parenchymal foci of hypercellularity in age-matched comparisons ($p<0.01$ in young infected versus young healthy; $p<0.0001$ in 12-month-old infected versus 12-month-old healthy; two-way ANOVA and Tukey's multiple comparisons test) (Fig 1C). Middle aged infected mice had ~30% more parenchymal inflammatory foci than young, infected mice ($p<0.0001$). We found few inflammatory foci in choroid plexus, ependyma, or attached meninges, indicating that in our model, infection with SARS-CoV-2 does not induce hypercellularity in blood-CSF barrier forming cells (Fig 1C). We did note that healthy aging increased perivascular inflammation in the meninges and ventricles ($p<0.01$) (Fig 1C). Thus, normal aging increases meningeal/ventricular (blood-meningeal barrier and blood-cerebrospinal fluid barrier) inflammation, whereas SARS-CoV-2 increases parenchymal (BBB) inflammation that is exacerbated by age.

We noted morphologic similarity between the perivascular hypercellularity after SARS-CoV-2 infection and after classic models for CNS autoimmune disease, in which T cell invasion of the CNS causes tissue destruction and motor/neuropsychiatric impairment (Lengfeld *et al.*, 2017; Lutz *et al.*, 2017). In neurotropic infections, CNS influx of virus-specific T cells is essential to control infection but also causes post-infectious cognitive dysfunction (Ai and Klein, 2020; Prasad and Lokensgard, 2019). We therefore asked whether SARS-CoV-2 respiratory infection increased CD3+ T cell infiltration of the brain in older mice. Indeed, we observed ~60% increase in CD3+ T cell count in brains of 12-month-old SARS-CoV-2 infected mice as compared with 2-month-old infected mice ($p<0.01$, two-way ANOVA and Dunnett's multiple comparisons test; Fig 1D-H). To determine whether the CNS-infiltrating T cells were associated with the BBB or blood-CSF barriers, we assessed T cell position in sections double immunostained for CD3 and Glut1 (Fig 1D-H). SARS-CoV-2 infection in 12-month-old-mice increased T cells proximal to parenchymal vessels ($p<0.001$) but not the ventricles ($p=0.8$) (Fig 1H).

We then assessed the neuroanatomic distribution of T cells in the CNS, to learn whether SARS-CoV-2 infection might cause inflammation in specifically vulnerable brain regions. Indeed, we observed a 4-fold increase in CD3+ T cell infiltration of the brainstem in SARS-CoV-2 infected 12-month-old mice as compared to younger infected mice ($p<0.001$, two-way ANOVA and Tukey's multiple comparisons test; Figure 4B). We observed a ~1.5-fold increase in olfactory bulb T cells in 12-month-old SARS-CoV-2 infected mice compared with age-matched controls ($p<0.05$), and a non-significant trend when compared with 2-month-old SARS-CoV-2 infected mice ($p=0.08$). No significant differences were noted in T cell number in cortex, hippocampus, thalamus, or cerebellum between 2-month-old and 12-month-old infected mice. Thus, we found that middle-age increases T cell CNS infiltration after SARS-CoV-2, with T cells in infected middle-aged mice primarily crossing the BBB in the brainstem and the olfactory bulb.

SARS-CoV-2 Viral measurements

We asked whether increased leukocyte infiltration of the CNS could be related to increased viral burden in the brain or in the lung. We therefore conducted RT-qPCR for SARS-CoV-2 viral RNA. We determined that at 4DPI, age did not significantly influence viral RNA burden in the lung (viral RNA geometric mean (±SD) for 2-month-old 6.1×10^4 (±9.7) versus 12-month-old adult 5.3×10^4 (±75.8) viral genomes/mg tissue; Fig 2B). Next, to determine if brainstem and olfactory bulb inflammation related to elevated local concentrations of virus or viral

materials, we measured SARS-CoV-2 RNA by RT-qPCR in central nervous system (CNS) tissues in 2-month-old and 12-month-old mice. Viral RNA was detected at similar levels between 2-month-old and 12-month-old in all assayed CNS regions: olfactory bulb, forebrain, cerebellum, brainstem, spinal cord (Fig. 2B). Geometric means for viral RNA in brain regions ranged from 11 to 349 viral genomes/mg tissue and did not significantly differ between brain region or between ages (non-parametric two-way ANOVA). Viral RNA was below limit of detection in blood, heart, kidney, liver, and spleen (n=5 per group, data not shown), indicating that there is no viremia at this time point in our model and further indicating that accumulation of viral RNA is specific to the lung and brain. These studies established that moderately advanced age does not increase SARS-CoV-2 RNA in the lung or brain in C57Bl/6 mice 4 days after nasal inoculation. We also assessed body weight as an indicator of overall health status. We found that 2-month-old adults maintained their weight while 12-month-old mice decreased body weight by an average of 10% at four days post inoculation (4DPI) (Fig 2A). This result is similar to previous reports in which 12-month-old BALBC mice experienced more severe morbidity and weight loss than 2-month-old BALBC mice after SARS-CoV-2 inoculation (Leist *et al.*, 2020). Thus, SARS-CoV-2 causes age-dependent morbidity in C57Bl/6 mice, but age is not an important factor in determining viral load in the brain.

SARS-CoV-2 transcellular BBB leakage to blood proteins

We asked whether inflammation could be related to vascular leakage. For this, we measured CNS accumulation of fibrinogen, a protein abundant in blood that is normally excluded from the brain by the actions of the BBB. Fibrinogen is highly pro-inflammatory, triggering demyelination, destruction of synapses, and cognitive impairment in neurological diseases(Merlini et al., 2019; Petersen et al., 2018). We found parenchymal accumulation of fibrinogen was significantly greater in infected mice as compared to age-matched vehicle controls (Fig 7A-B). Two-month-old infected mice had approximately doubled fibrinogen area immunoreactivity in the brainstem reticular formation as compared with age-matched healthy mice ($p<0.001$, one-way ANOVA, Sidak's multiple comparisons test). 12-month-old infected mice had approximately 3-fold greater fibrinogen area immunoreactivity in brainstem as compared with 12-month-old healthy mice ($p<0.0001$). Infected 12-month-olds had more fibrinogen area immunoreactivity than infected 2-month-olds ($p<0.01$). We then corroborated these results using Western blot of brainstem homogenate (Fig 7C-D). 12-

month-old infected mice had more brainstem fibrinogen than age-matched vehicle ($p<0.001$, one-way ANOVA and Sidak's multiple comparisons test). Thus, age exacerbates BBB leakage caused by SARS-CoV-2 infection.

BBB permeability occurs through two pathways: movement through the spaces in between adjacent endothelial cells through disrupted tight junctions, and through the cytoplasm of the endothelial cell (transcytosis) (Mapunda *et al.*, 2022). Caveolin-1 is a signaling and scaffolding molecule that can promote transcellular BBB permeability(Knowland *et al.*, 2014; Lengfeld *et al.*, 2017; Lutz *et al.*, 2017; Martin *et al.*, 2022) and that increases BBB permeability with age (Guérit et al., 2020; Yang et al., 2020). We assessed Caveolin-1 and tight junction proteins. We measured mean fluorescence intensity of Caveolin-1 immunostaining in brainstem sections (Fig 8A-D). Caveolin-1 underwent significant age-dependent upregulation in healthy mice ($p<0.05$, one-way ANOVA and Sidak's multiple comparisons test). Furthermore, SARS-CoV-2 infection significantly upregulated Caveolin-1 in the 12-month-old mice ($p<0.01$ as compared with aged healthy; $p<0.001$ as compared with 2-month-old SARS-CoV-2 infected mice). We then sought to confirm and extend these findings by Western blotting of microdissected brainstem. By Western blotting, we observed a similar trend toward increased Caveolin-1 with age and infection (Fig 4F-G). We also investigated whether age and SARS-CoV-2 would downregulate tight junction proteins, potentially contributing to paracellular BBB leakage. By Western blot, we did not observe significant differences in tight junction proteins Occludin or Claudin5 (Fig 4F, H, I). However, SARS-CoV-2 infection decreased brainstem ZO-1, a protein stably linking junctional proteins to the cytoskeleton to restrict macromolecular permeability (Otani et al., 2019) (Fig 4F, J). These results suggest that age exacerbates transcellular BBB leakage caused by SARS-CoV-2 infection.

Wnt/β-catenin downregulation in aging and infection

Previous work has established that Wnt ligands Wnt7a/7b act on brain endothelial cells to suppress transcellular and paracellular BBB permeability during late embryogenesis/early postnatal life (Daneman *et al.*, 2009; Liebner *et al.*, 2008; Stenman *et al.*, 2008). Similarly, Wnt ligands are required for the maintenance of BBB function in the adult (Guérit *et al.*, 2020; Martin *et al.*, 2022; Tran *et al.*, 2016). We previously showed that in autoimmune neuroinflammation, Wnt3 acting on BBB endothelial cells is required for suppression of the BBB

transcytosis protein Caveolin-1. Loss of the canonical Wnt/β-catenin pathway in brain endothelial cells induced dramatic Caveolin-1-dependent transcellular BBB permeability, increased CD3 T cell infiltration, and neuroinflammation. Both Wnt7a and Wnt3 are canonical Wnt ligands that exert their BBB-stabilizing effects through the transcriptional activity of the β-catenin/TCF/LEF complex. We therefore investigated whether the increased Caveolin-1 levels and BBB permeability in middle-aged mice infected with SARS-CoV-2 could be due to Wnt/β-catenin dysregulation. We hypothesized that decreased canonical Wnts would correlate with impaired BBB function in SARS-CoV-2 infection, especially in middle-aged mice. If true, this would provide a potential mechanistic basis for age-related declines in BBB function. Since SARS-CoV-2 neuroinflammatory changes and cerebrovascular inflammation are most severe in the brainstem, we conducted QPCR analysis of a panel of Wnt ligands in microdissected brainstem from 2-month-old vehicle, 2-month-old SARS-CoV-2, 12-month-old vehicle, and 12-month-old SARS-CoV-2 infected mice. Indeed, we found that Wnt3 was reduced ~80% (Fig 5A, $p<0.01$; one-way ANOVA and Sidak's multiple comparisons test) and Wnt7a was reduced ~50% by age (Fig 5B, $p<0.05$). Infection also suppressed Wnt7a (Fig 5B $p<0.05$). No significant changes were noted in Wnt7b (Fig 5C). Interestingly, no significant changes were noted in non-canonical Wnt5a and Wnt5b, which function independently of TCF/LEF transcriptional activity (Fig 5D-E). Finally, to determine whether downregulation of canonical Wnts resulted in measurable changes in transcription, we measured the TCF/LEF transcriptional target Apcdd1(Shimomura et al., 2010). Apcdd1 was reduced in 12-month-old mouse brainstem ($p<0.05$) but not significantly changed by infection (Fig 5F). Thus, the Wnt/β-catenin pathway is dysregulated in regions of neuroinflammation in middle-aged mice.

SARS-COV-2 acute gliosis

We then assessed immunoreactivity for the astrocyte intermediate filament protein GFAP, a sensitive indicator of neuroinflammation. We first assessed the impact of healthy aging on astrocytic activation. Aging was associated with 3-fold increased GFAP in brainstem ($p<0.001$ one way ANOVA with Sidak's multiple comparisons test) and ~2-fold in hippocampus ($p<0.05$) (Fig 6A, B, D, E). Age did not significantly increase GFAP in olfactory bulb (Fig 5C, F). We assessed whether infection increased GFAP in age-matched comparisons. SARS-COV-2 infection did not increase GFAP in 2-month-old mice (Fig 5A-F). In 12-month-old-mice, infection did strikingly increase GFAP in brainstem (3.6% versus 2.0%, $p<0.001$), but not in olfactory bulb

or hippocampus (Fig 5A-F). Thus, we observed neuroanatomically specific patterns of astrocytic response to SARS-CoV-2 infection in 12-month-old mice.

We measured morphological microglial responses to infection. Previous studies have documented microglial activation and monocyte/macrophage CNS infiltration in COVID-19 (Fernández-Castañeda et al., 2022; Klein et al., 2021; Lee et al., 2021; Matschke et al., 2020; Reichard et al., 2020; Schwabenland *et al.*, 2021; Thakur et al., 2021). Indeed, macrophages infected with SARS-CoV-2 die by inflammatory pyroptotic death (Sefik et al., 2022). We assessed Iba1, a calcium binding protein expressed in microglia and macrophages which is profoundly upregulated in inflammation. We observed that SARS-COV-2 infection doubled area of Iba1 immunoreactivity in brainstem and olfactory bulb in age-matched comparisons (Fig 7A-F, $p<0.001$, ANOVA with Sidak's multiple comparisons test). The combined effect of age and infection also significantly increased Iba1 immunoreactivity (Fig 7A, D, $p<0.05$ for aged infected versus young infected brainstem). In hippocampus CA1, infection in 2-month-old mice but not 12-month-old mice significantly increased Iba1 reactivity ($p<0.05$; ANOVA with Sidak's test). Moreover, microglial morphology changed in response to infection. Microglia in infected brains had fewer complex processes and enlarged soma (Fig 7A, B). Some vessels contained large, ameboid Iba1+ cells embedded within the vessel wall, giving the appearance of perivascular engraftment of peripheral monocytes (Figure 7G). Similarly, we consistently found numerous small round Iba1+ profiles underlying the 4th ventricle in the pontine central gray (Figure 7H). Brainstem reticular formation contained microglial nodules (Fig 7I). Thus, microglia undergo morphologic evidence of reactivity in a region-specific manner in response to respiratory infection with SARS-COV-2 in aged mice.

SARS-CoV-2 infection causes cognitive impairment and neuropsychiatric abnormalities

Because COVID-19 and Long COVID are associated with cognitive and neuropsychiatric decline, and because we observed that age exacerbated neuroinflammation and BBB disruption after infection, we assayed cognitive and neuropsychiatric behaviors in aged SARS-CoV-2 infected mice. We first conducted novel object recognition (NOR), a well-established assay for learning and memory. We conducted familiarization at 3DPI and NOR at 4DPI (24h inter-session interval). Mice that spend more than 50% of their exploration time with the novel object are considered to "remember" the familiar object and prefer the novel object. As expected, 2-month-old healthy mice preferred the novel object (Fig 8A-B). Importantly, we found that 2-month-old mice infected with SARS-CoV-2 were impaired in this assay of learning and memory (Fig 8B). 2-month-old vehicle

treated mice attended to the novel object 61.2% of the time whereas infected 2-month-old mice attended to the novel object 48.4% of the time (Fig 8A-B, $p<0.001$; two-way ANOVA and Sidak's multiple comparisons test, n=5-8 mice per group). NOR decreased with advancing age (12-month vehicle-treated mice, mean 51.5%, $p<0.05$ versus 2-month vehicle-treated). Healthy 12-month-old and infected 12-month-old mice did not favor the novel object with more time than accounted for by random chance (50%). We also considered that mice demonstrating generalized sickness behavior might be lethargic and non-exploratory. To avoid potential confounding effects of inactivity, exclusion criteria were failure to explore objects for at least 0.5% of the trial time. Two infected mice were excluded from the NOR assay. Importantly, however, no significant differences were noted in the overall duration of object exploration between the infected and vehicle-treated mice (Fig 8C). This indicates that NOR test is a valid instrument for assessing cognition in SARS-CoV-2 infected mice. These results establish that respiratory SARS-CoV-2 infection decreased cognitive performance.

We then asked whether infection impaired simple locomotion and complex motor tasks. 2-month-old mice inoculated with SARS-CoV-2 trended toward hyperkinesia compared with uninfected 2-month-old mice (>1.5-fold greater velocity and 1.5-fold greater distance traveled in the open field, Fig 8D-E). In contrast, 12-month-old mice inoculated with SARS-CoV-2 traveled less distance and moved more slowly in an open field (~2-fold reduction in velocity and distance traveled, $p<0.001$, one-way ANOVA and Sidak's multiple comparisons test) (Fig 8D-E). Open field locomotion is influenced by voluntary and involuntary behaviors reflecting cerebral and brainstem circuity. To gain more insight into the motor deficit, we measured bradykinesia with the pole descent assay (Fig 8F). The pole-descent assay integrates complex motor circuits and is disrupted in models of Parkinson's disease, other neuropsychiatric disorders, and after traumatic brain injury (Ogawa et al., 1985). 12-month-old mice inoculated with SARS-COV-2 had significantly greater latency to descend the pole (mean 14.7 second descent) as compared to 12-month-old mice treated with vehicle (mean 7.6 second descent, $p<0.0001$, one way ANOVA with Sidak's multiple comparisons test) or to 2-month-old mice inoculated with SARS-COV-2 (5.9 second descent, $p<0.0001$ one way ANOVA with Sidak's multiple comparisons test) (Fig 8G). Interestingly, no defects were noted in a composite phenotypic battery for cerebellar ataxia (Guyenet *et al.*, 2010) incorporating ledge test, hindlimb clasping, gait, or kyphosis (not shown). This suggests that cerebellum circuity may be spared in SARS-CoV-2 infection in all ages. In summary, SARS-CoV-2 infection in middle-aged

mice but not young adult mice results in severe bradykinesia, indicating that age strongly influences motor deficits in SARS-CoV-2 infection.

Neuropsychiatric disorders are epidemiologically but not mechanistically linked with COVID-19 and Long-COVID. Neurocognitive, psychiatric, and motor/sensory disorders are increased after COVID-19, especially in middle-aged and advanced age adults (Graham *et al.*, 2021; Guo *et al.*, 2022; Nalbandian *et al.*, 2021; Taquet *et al.*, 2021). To gain insight into how SARS-CoV-2 infection might modulate neural control of behavior, we analyzed self-grooming behavior in the open field videos (Fig 8H-I). Self-grooming in mice is an innate behavior coordinately regulated by cerebral modification of brainstem chains of motor activities. Mouse self-grooming is altered in diverse models of neuropsychiatric disorders including anxiety disorder, obsessive-compulsive disorder, autism spectrum, Parkinson's disease, and Huntington's disease (Feusner et al., 2009; Kalueff *et al.*, 2016). We observed striking grooming changes in infected 12-month-old mice (Fig 8H-I). 12-month-old mice inoculated with SARS-COV-2 nearly doubled grooming bout duration (mean 8.0 seconds/bout) as compared with 12-month-old vehicle treated mice (4.9 seconds, $p<0.05$, one-way ANOVA, Sidak's multiple comparison test) or 2-month-old infected mice (3.7 seconds, $p<0.05$, one-way ANOVA, Sidak's multiple comparison test) (Fig 8H). 2-month-old infected and uninfected mice had indistinguishable grooming duration. We then measured grooming initiations (Fig 8I). Again, we noted age-dependent modification of grooming in infected mice. 12-month-old infected mice initiated grooming fewer times (mean 2.9) than did 2-month-old infected mice (mean 9.8; $p<0.01$, Kruskal-Wallis with Dunn's multiple comparisons test) (Fig 2I). Cumulative grooming duration was similar between groups (not shown). In summary, SARS-CoV-2 infection in middle-aged mice but not young adult mice induced prolonged complex, repetitive, self-directed stereotypical behavior.

Discussion

To our knowledge, we have for the first time used a small animal model to experimentally test the impact of age on the neuropathology of SARS-CoV-2. We recapitulate in mice key features of COVID-19 neuropathology and neurobehavioral disorders in patients, and we advance these findings by providing well-controlled

experimental evidence that moderately advanced age worsens the neuroinflammatory response due to dysregulation of Wnt/β-catenin signaling and BBB permeability.

Following previously published life-stage equivalencies, we considered two-month-old young adult C57Bl/6 mice as human life-stage equivalent 16-20 years old, and 12-month-old middle-aged C57Bl/6 mice as human life-stage equivalent to 38-47 years old (Flurkey et al., 2007). We inoculated mice with SARS-CoV-2 (MA10) via droplet inhalation, resulting in pulmonary infection. In humans, neurological and neuropsychiatric disorders occur after acute infection, when viral replication is no longer detected in the respiratory tract (Nalbandian *et al.*, 2021; Taquet *et al.*, 2021). We selected 4 days post-inoculation as a subacute timepoint, after the peak of viral replication in the lung (Leist *et al.*, 2020), to measure neurologic and neuropathologic outcomes. We did not measure active viral replication. Age did not influence the amount of viral RNA in the lung. We detected viral RNA in multiple CNS tissues, but we did not detect infectious viral particles in these sites. Moreover, we detected equivalent levels of SARS-CoV-2 RNA in middle-aged and young mouse CNS, demonstrating that pathogen-associated molecular patterns are highly expressed in the brain after SARS-CoV-2 infection and do not differ by age. Our interpretation is that age critically influences the cerebrovascular and neuroimmunological response to encounters with virus and viral pathogen associated molecular patterns. Concordantly, while microglia upregulated Iba1 and adopted ameboid morphology in response to SARS-CoV-2 in all ages, the cerebrovascular inflammation was much worse in the aged. Specifically, SARS-CoV-2 inoculation of middle-aged mice significantly increased perivascular inflammation, T cell infiltration, BBB permeability, induction of the BBB transcytosis protein Caveolin-1, with downregulation of ZO-1 and no apparent changes to tight junction proteins. Cerebrovascular Caveolin-1 increases with aging (Guérit *et al.*, 2020; Martin *et al.*, 2022). Indeed, previous work established that age-dependent increases in Caveolin-1 are pathologic by increasing brain uptake of toxic macromolecules from the blood, at the expense of growth factors(Yang *et al.*, 2020). Thus, SARS-CoV-2 infection exacerbated age-related transcellular BBB leakage.

SARS-CoV-2 neuropathology caused striking age-dependent behavioral abnormalities reminiscent of Long COVID cognitive and neuropsychiatric disorders. In younger mice, SARS-COV-2 infection disrupted learning and memory. In older mice, SARS-COV-2 infection induced Parkinsonian-like bradykinesia (Ogawa *et al.*, 1985). We also observed hypokinesia and spontaneous obsessive-compulsive behavior in older infected mice. These divergent manifestations of SARS-CoV-2 infection illustrate distinct neurologic and neuropsychiatric

vulnerabilities across the lifespan. SARS-CoV-2 infection thus provides a valuable experimental model for the impact of age on cognitive impairment, disorders of anxiety or compulsivity, and sensory motor deficit observed in some LongCOVID patients (Taquet *et al.*, 2021). Future work will be required to identify potential therapeutic strategies that could ameliorate some of the debilitating features of Long COVID.

Brainstem and olfactory bulb emerged as sites of special vulnerability to COVID neuropathology in our middle-aged mice, like in patients (Lee *et al.*, 2021; Matschke *et al.*, 2020; Thakur *et al.*, 2021). Our model of "natural infection" relies upon the endogenous, unmanipulated expression of SARS-CoV-2 receptors and coreceptors in the host. Our results are therefore distinct from K18-driven overexpression of human ACE2 in mice, in which respiratory inoculation yields extreme neurotropism and viral encephalitis (Fumagalli et al., 2022). Our findings in young adult SARS-CoV-2 (MA10) inoculated mice are more consistent with cerebrovascular inflammation and brainstem demyelination in human ACE-2 engineered mice or in hamsters inoculated with SARS-CoV-2 (WA1) strain(Fernández-Castañeda *et al.*, 2022; Klein *et al.*, 2021) and in non-human primate SARS-CoV-2 infection(Rutkai et al., 2022). Our findings of BBB leakage are also in accord with other studies documenting BBB damage after systemic infection in rodents (Zhang *et al.*, 2021), after brain endothelial interaction with SARS-CoV-2 infectious virus or viral PAMPs (Krasemann *et al.*, 2022; Rauti *et al.*, 2021; Reynolds and Mahajan, 2021; Wenzel *et al.*, 2021), or in umbilical vein endothelial cells overexpressing individual viral genes (Rauti *et al.*, 2021). Similar to our results, respiratory SARS-CoV-2 infection in hamsters caused BBB leakage despite no loss of tight junction proteins(Zhang *et al.*, 2021), suggesting that trans-endothelial permeability including caveolar-dependent transcytosis might drive BBB leakage in COVID-19.

Age-related changes in the brain and cerebrovasculature may render aged individuals more susceptible to parainfectious neuroinflammation. Indeed, age strongly influences cerebrovascular injury, inflammation, and neurodegenerative disease(Iadecola *et al.*, 2020; Merlini *et al.*, 2019; Tai et al., 2016; Thompson et al., 2018; Zlokovic et al., 2020). Aging of the immune system and the nervous system contribute to increased SARS-CoV-2 morbidity and mortality (Arthur et al., 2021; Bartleson et al., 2021; Bastard, 2022; Brodin, 2021). Our data are consistent with many previous reports indicating that aging primes microglia and astrocytes for greater inflammation in response to insult (Boisvert et al., 2018; Clarke et al., 2018; Suda et al., 2021), which could exacerbate BBB leakage and T cell infiltration in SARS-CoV-2 infection. For example, glia in the aged brain profoundly upregulate chemokines important for leukocyte recruitment into the brain as well as increased

antigen presentation activity(Atkinson et al., 2022; Boisvert *et al.*, 2018; Clarke *et al.*, 2018; Peferoen et al., 2016; Suda *et al.*, 2021). Age is also known to decrease astrocytic secretion of Wnt ligands and thereby increase BBB transcellular permeability (Guérit *et al.*, 2020). Reactive microglial and macrophages present antigen and restimulate T cells in CNS in COVID-19 (Schwabenland *et al.*, 2021). CNS-infiltrating T cells directly damage neurons, axons, and myelin to cause neurological impairment (Ai and Klein, 2020; Mapunda *et al.*, 2022; Prasad and Lokensgard, 2019). Concordantly, T-cell mediated neuroinflammation is exacerbated in middle-aged mice(Atkinson *et al.*, 2022; Peferoen *et al.*, 2016). Therefore age-dependent parainfectious brainstem and olfactory bulb microglial reactivity in our model contributes to the age-dependent focal T cell infiltration and neuropsychiatric signs.

Finally, we identified Wnt/β-catenin signaling as a potential mechanistic basis relating age to severity of NeuroCOVID. Previous work has established, in human and in mouse, that Wnt7a/7b is required for CNS angiogenesis and that Wnt3/3a suppresses inflammatory T cell migration across the cerebrovasculature (Daneman *et al.*, 2009; Guérit *et al.*, 2020; Lengfeld *et al.*, 2017; Liebner *et al.*, 2008; Martin *et al.*, 2022; Stenman *et al.*, 2008; Tran *et al.*, 2016). Our data suggest that the resiliency of young adults to SARS-CoV-2 is related to robust canonical Wnt activity. Conversely age-dependent loss of Wnt7a and Wnt3a facilitates inflammatory leukocyte entry into the brain after SARS-CoV-2 infection. We suggest that BBB permeability in aged infected mice is due to loss of Wnt3 and Wnt7a suppression of Caveolin-1, which could in fact exacerbate inflammation by enhancing delivery of viral material across the BBB. Thus, our data suggest that loss of protective Wnt/β-catenin in the aging brain creates vulnerability to NeuroCOVID.

Furthermore, while in this study we focus on the impact of age on SARS-CoV-2 neuropathology, open questions remain regarding the long-term impact of SARS-CoV-2 on aging. For example, gliosis, vascular rarefaction, and white matter damage caused by SARS-CoV-2 infection are reminiscent of cerebrovascular changes in Alzheimer's disease and vascular cognitive impairment and dementia (VCID) (Tai *et al.*, 2016; Zlokovic *et al.*, 2020). Indeed, brain endothelial cell transcriptomic signatures are highly conserved between COVID-19 and Alzheimer's disease(Zhou et al., 2021). Cerebrovascular damage caused by SARS-CoV-2 infection could induce or accelerate VCID. In this regard it is particularly troubling that new-onset dementia is diagnosed in 1.6% of adults 65 years and older in just the first three months after SARS-CoV-2 infection, or 2.4 times more common than after other acute health events (Taquet *et al.*, 2021). The cumulative consequences

of increased neuropsychiatric disease and dementia after the COVID-19 pandemic could be staggering in future years.

In summary, we showed that middle-aged adults experience more severe SARS-CoV-2 neuroinflammation and neurobehavioral impairment than young adults, due in part to increased Caveolin-1 BBB permeability and loss of protective Wnt signaling. Our data help explain why middle-aged individuals have more neuropathological and neuropsychiatric sequalae to COVID-19. These findings are early steps in the identification of potential new therapeutic strategies for enhancing cerebrovascular function to increase resiliency of the aging brain.

Acknowledgements

This work was supported by the Department of Defense Congressionally Directed Medical Research Program Award MS200290 and National Institute of Health KL2TR002002 to SEL.

Literature Cited

1. Ai, S., and Klein, R.S. (2020). Update on T cells in the virally infected brain: friends and foes. Current opinion in neurology *33*, 405-412. 10.1097/wco.0000000000000825.

2. Ameres, M., Brandstetter, S., Toncheva, A.A., Kabesch, M., Leppert, D., Kuhle, J., and Wellmann, S. (2020). Association of neuronal injury blood marker neurofilament light chain with mild-to-moderate COVID-19. Journal of neurology *267*, 3476-3478. 10.1007/s00415-020-10050-y.

3. Arthur, L., Esaulova, E., Mogilenko, D.A., Tsurinov, P., Burdess, S., Laha, A., Presti, R., Goetz, B., Watson, M.A., Goss, C.W., et al. (2021). Cellular and plasma proteomic determinants of COVID-19 and non-COVID-19 pulmonary diseases relative to healthy aging. Nature Aging *1*, 535-549. 10.1038/s43587-021-00067-x.

4. Atkinson, J.R., Jerome, A.D., Sas, A.R., Munie, A., Wang, C., Ma, A., Arnold, W.D., and Segal, B.M. (2022). Biological aging of CNS-resident cells alters the clinical course and immunopathology of autoimmune demyelinating disease. JCI insight. 10.1172/jci.insight.158153.

5. Bartleson, J.M., Radenkovic, D., Covarrubias, A.J., Furman, D., Winer, D.A., and Verdin, E. (2021). SARS-CoV-2, COVID-19 and the Ageing Immune System. Nat Aging *1*, 769-782. 10.1038/s43587-021-00114-7.

6. Bastard, P. (2022). Why do people die from COVID-19? Science *375*, 829-830. 10.1126/science.abn9649.

7. Boisvert, M.M., Erikson, G.A., Shokhirev, M.N., and Allen, N.J. (2018). The Aging Astrocyte Transcriptome from Multiple Regions of the Mouse Brain. Cell reports *22*, 269-285. 10.1016/j.celrep.2017.12.039.

8. Brodin, P. (2021). Immune determinants of COVID-19 disease presentation and severity. Nat Med *27*, 28-33. 10.1038/s41591-020-01202-8.

9. Chioh, F.W.J., Fong, S.-W., Young, B.E., Wu, K.-X., Siau, A., Krishnan, S., Chan, Y.-H., Carissimo, G., Teo, L.L.Y., Gao, F., et al. (2021). Convalescent COVID-19 patients are susceptible to endothelial dysfunction due to persistent immune activation. eLife *10*, e64909. 10.7554/eLife.64909.

10. Clarke, L.E., Liddelow, S.A., Chakraborty, C., Münch, A.E., Heiman, M., and Barres, B.A. (2018). Normal aging induces A1-like astrocyte reactivity. Proceedings of the National Academy of Sciences of the United States of America *115*, E1896-e1905. 10.1073/pnas.1800165115.

11. Daneman, R., Agalliu, D., Zhou, L., Kuhnert, F., Kuo, C.J., and Barres, B.A. (2009). Wnt/beta-catenin signaling is required for CNS, but not non-CNS, angiogenesis. Proceedings of the National Academy of Sciences of the United States of America *106*, 641-646.

12. Dinnon, K.H., 3rd, Leist, S.R., Schäfer, A., Edwards, C.E., Martinez, D.R., Montgomery, S.A., West, A., Yount, B.L., Jr., Hou, Y.J., Adams, L.E., et al. (2020). A mouse-adapted model of SARS-CoV-2 to test COVID-19 countermeasures. Nature *586*, 560-566. 10.1038/s41586-020-2708-8.

13. Fernández-Castañeda, A., Lu, P., Geraghty, A.C., Song, E., Lee, M.H., Wood, J., Yalçın, B., Taylor, K.R., Dutton, S., Acosta-Alvarez, L., et al. (2022). Mild respiratory SARS-CoV-2 infection can cause multi-lineage cellular dysregulation and myelin loss in the brain. bioRxiv. 10.1101/2022.01.07.475453.

14. Feusner, J.D., Hembacher, E., and Phillips, K.A. (2009). The mouse who couldn't stop washing: pathologic grooming in animals and humans. CNS Spectr *14*, 503-513. 10.1017/s1092852900023567.

15. Flurkey, K., Currer, J., and Harrison, D. (2007). The Mouse in Aging Research. In The Mouse in Biomedical Research 2nd Edition., F. JG, ed. (American College Laboratory Animal Medicine (Elsevier)), pp. 637–672.

16. Fumagalli, V., Ravà, M., Marotta, D., Di Lucia, P., Laura, C., Sala, E., Grillo, M., Bono, E., Giustini, L., Perucchini, C., et al. (2022). Administration of aerosolized SARS-CoV-2 to K18-hACE2 mice uncouples respiratory infection from fatal neuroinvasion. Sci Immunol *7*, eabl9929. 10.1126/sciimmunol.abl9929.

17. Graham, E.L., Clark, J.R., Orban, Z.S., Lim, P.H., Szymanski, A.L., Taylor, C., DiBiase, R.M., Jia, D.T., Balabanov, R., Ho, S.U., et al. (2021). Persistent neurologic symptoms and cognitive dysfunction in non-hospitalized Covid-19 "long haulers". Ann Clin Transl Neurol *8*, 1073-1085. 10.1002/acn3.51350.

18. Guérit, S., Fidan, E., Macas, J., Czupalla, C.J., Figueiredo, R., Vijikumar, A., Yalcin, B.H., Thom, S., Winter, P., Gerhardt, H., et al. (2020). Astrocyte-derived Wnt growth factors are required for endothelial blood-brain barrier maintenance. Prog Neurobiol, 101937. 10.1016/j.pneurobio.2020.101937.

19. Guo, P., Benito Ballesteros, A., Yeung, S.P., Liu, R., Saha, A., Curtis, L., Kaser, M., Haggard, M.P., and Cheke, L.G. (2022). COVCOG 1: Factors Predicting Physical, Neurological and Cognitive Symptoms in Long COVID in a Community Sample. A First Publication From the COVID and Cognition Study. Front Aging Neurosci *14*, 804922. 10.3389/fnagi.2022.804922.

20. Guyenet, S.J., Furrer, S.A., Damian, V.M., Baughan, T.D., La Spada, A.R., and Garden, G.A. (2010). A simple composite phenotype scoring system for evaluating mouse models of cerebellar ataxia. J Vis Exp. 10.3791/1787.

21. Iadecola, C., Anrather, J., and Kamel, H. (2020). Effects of COVID-19 on the Nervous System. Cell *183*, 16-27.e11. 10.1016/j.cell.2020.08.028.

22. Kalueff, A.V., Stewart, A.M., Song, C., Berridge, K.C., Graybiel, A.M., and Fentress, J.C. (2016). Neurobiology of rodent self-grooming and its value for translational neuroscience. Nature reviews *17*, 45-59. 10.1038/nrn.2015.8.

23. Klein, R., Soung, A., Sissoko, C., Nordvig, A., Canoll, P., Mariani, M., Jiang, X., Bricker, T., Goldman, J., Rosoklija, G., et al. (2021). COVID-19 induces neuroinflammation and loss of hippocampal neurogenesis. Res Sq. 10.21203/rs.3.rs-1031824/v1.

24. Knowland, D., Arac, A., Sekiguchi, K.J., Hsu, M., Lutz, S.E., Perrino, J., Steinberg, G.K., Barres, B.A., Nimmerjahn, A., and Agalliu, D. (2014). Stepwise recruitment of transcellular and paracellular pathways underlies blood-brain barrier breakdown in stroke. . Neuron *82*, 1-15.

25. Krasemann, S., Haferkamp, U., Pfefferle, S., Woo, M.S., Heinrich, F., Schweizer, M., Appelt-Menzel, A., Cubukova, A., Barenberg, J., Leu, J., et al. (2022). The blood-brain barrier is dysregulated in COVID-19 and serves as a CNS entry route for SARS-CoV-2. Stem Cell Reports. 10.1016/j.stemcr.2021.12.011.

26. Lee, M.H., Perl, D.P., Nair, G., Li, W., Maric, D., Murray, H., Dodd, S.J., Koretsky, A.P., Watts, J.A., Cheung, V., et al. (2021). Microvascular Injury in the Brains of Patients with Covid-19. N Engl J Med *384*, 481-483. 10.1056/NEJMc2033369.

27. Leist, S.R., Dinnon, K.H., 3rd, Schäfer, A., Tse, L.V., Okuda, K., Hou, Y.J., West, A., Edwards, C.E., Sanders, W., Fritch, E.J., et al. (2020). A Mouse-Adapted SARS-CoV-2 Induces Acute Lung Injury and Mortality in Standard Laboratory Mice. Cell *183*, 1070-1085.e1012. 10.1016/j.cell.2020.09.050.

28. Lengfeld, J.E., Lutz, S.E., Smith, J.R., Diaconu, C., Scott, C., Kofman, S.B., Choi, C., Walsh, C.M., Raine, C.S., Agalliu, I., and Agalliu, D. (2017). Endothelial Wnt/beta-catenin signaling reduces immune cell infiltration in multiple sclerosis. Proceedings of the National Academy of Sciences of the United States of America *114*, E1168-e1177. 10.1073/pnas.1609905114.

29. Liebner, S., Corada, M., Bangsow, T., Babbage, J., Taddei, A., Czupalla, C.J., Reis, M., Felici, A., Wolburg, H., Fruttiger, M., et al. (2008). Wnt/beta-catenin signaling controls development of the blood-brain barrier. J Cell Biol *183*, 409-417.

30. Lutz, S.E., Smith, J.R., Kim, D.H., Olson, C.V.L., Ellefsen, K., Bates, J.M., Gandhi, S.P., and Agalliu, D. (2017). Caveolin1 Is Required for Th1 Cell Infiltration, but Not Tight Junction Remodeling, at the Blood-Brain Barrier in Autoimmune Neuroinflammation. Cell reports *21*, 2104-2117. 10.1016/j.celrep.2017.10.094.

31. Mapunda, J.A., Tibar, H., Regragui, W., and Engelhardt, B. (2022). How Does the Immune System Enter the Brain? Frontiers in immunology *13*, 805657. 10.3389/fimmu.2022.805657.

32. Martin, M., Vermeiren, S., Bostaille, N., Eubelen, M., Spitzer, D., Vermeersch, M., Profaci, C.P., Pozuelo, E., Toussay, X., Raman-Nair, J., et al. (2022). Engineered Wnt ligands enable blood-brain barrier repair in neurological disorders. Science *375*, eabm4459. 10.1126/science.abm4459.

33. Matschke, J., Lütgehetmann, M., Hagel, C., Sperhake, J.P., Schröder, A.S., Edler, C., Mushumba, H., Fitzek, A., Allweiss, L., Dandri, M., et al. (2020). Neuropathology of patients with COVID-19 in Germany: a post-mortem case series. The Lancet. Neurology *19*, 919-929. 10.1016/s1474-4422(20)30308-2.

34. Merlini, M., Rafalski, V.A., Rios Coronado, P.E., Gill, T.M., Ellisman, M., Muthukumar, G., Subramanian, K.S., Ryu, J.K., Syme, C.A., Davalos, D., et al. (2019). Fibrinogen Induces Microglia-Mediated Spine Elimination and Cognitive Impairment in an Alzheimer's Disease Model. Neuron *101*, 1099-1108.e1096. 10.1016/j.neuron.2019.01.014.

35. Nalbandian, A., Sehgal, K., Gupta, A., Madhavan, M.V., McGroder, C., Stevens, J.S., Cook, J.R., Nordvig, A.S., Shalev, D., Sehrawat, T.S., et al. (2021). Post-acute COVID-19 syndrome. Nature medicine *27*, 601-615. 10.1038/s41591-021-01283-z.

36. Ogawa, N., Hirose, Y., Ohara, S., Ono, T., and Watanabe, Y. (1985). A simple quantitative bradykinesia test in MPTP-treated mice. Res Commun Chem Pathol Pharmacol *50*, 435-441.

37. Otani, T., Nguyen, T.P., Tokuda, S., Sugihara, K., Sugawara, T., Furuse, K., Miura, T., Ebnet, K., and Furuse, M. (2019). Claudins and JAM-A coordinately regulate tight junction formation and epithelial polarity. J Cell Biol *218*, 3372-3396. 10.1083/jcb.201812157.

38. Parisi, G.F., Diaferio, L., Brindisi, G., Indolfi, C., Umano, G.R., Klain, A., Marchese, G., Ghiglioni, D.G., Zicari, A.M., Marseglia, G.L., and Miraglia Del Giudice, M. (2021). Cross-Sectional Survey on Long Term Sequelae of Pediatric COVID-19 among Italian Pediatricians. Children (Basel) *8*. 10.3390/children8090769.

39. Peferoen, L.A., Breur, M., van de Berg, S., Peferoen-Baert, R., Boddeke, E.H., van der Valk, P., Pryce, G., van Noort, J.M., Baker, D., and Amor, S. (2016). Ageing and recurrent episodes of neuroinflammation promote progressive experimental autoimmune encephalomyelitis in Biozzi ABH mice. Immunology *149*, 146-156. 10.1111/imm.12644.

40. Pellegrini, L., Albecka, A., Mallery, D.L., Kellner, M.J., Paul, D., Carter, A.P., James, L.C., and Lancaster, M.A. (2020). SARS-CoV-2 Infects the Brain Choroid Plexus and Disrupts the Blood-CSF Barrier in Human Brain Organoids. Cell stem cell *27*, 951-961.e955. 10.1016/j.stem.2020.10.001.

41. Petersen, M.A., Ryu, J.K., and Akassoglou, K. (2018). Fibrinogen in neurological diseases: mechanisms, imaging and therapeutics. Nature reviews *19*, 283-301. 10.1038/nrn.2018.13.

42. Prasad, S., and Lokensgard, J.R. (2019). Brain-Resident T Cells Following Viral Infection. Viral immunology *32*, 48-54. 10.1089/vim.2018.0084.

43. Rauti, R., Shahoha, M., Leichtmann-Bardoogo, Y., Nasser, R., Paz, E., Tamir, R., Miller, V., Babich, T., Shaked, K., Ehrlich, A., et al. (2021). Effect of SARS-CoV-2 proteins on vascular permeability. eLife *10*. 10.7554/eLife.69314.

44. Reichard, R.R., Kashani, K.B., Boire, N.A., Constantopoulos, E., Guo, Y., and Lucchinetti, C.F. (2020). Neuropathology of COVID-19: a spectrum of vascular and acute disseminated encephalomyelitis (ADEM)-like pathology. Acta Neuropathol *140*, 1-6. 10.1007/s00401-020-02166-2.

45. Reynolds, J.L., and Mahajan, S.D. (2021). SARS-COV2 Alters Blood Brain Barrier Integrity Contributing to Neuro-Inflammation. J Neuroimmune Pharmacol *16*, 4-6. 10.1007/s11481-020-09975-y.

46. Rutkai, I., Mayer, M.G., Hellmers, L.M., Ning, B., Huang, Z., Monjure, C.J., Coyne, C., Silvestri, R., Golden, N., Hensley, K., et al. (2022). Neuropathology and virus in brain of SARS-CoV-2 infected non-human primates. Nature communications *13*, 1745. 10.1038/s41467-022-29440-z.

47. Schwabenland, M., Salié, H., Tanevski, J., Killmer, S., Lago, M.S., Schlaak, A.E., Mayer, L., Matschke, J., Püschel, K., Fitzek, A., et al. (2021). Deep spatial profiling of human COVID-19 brains reveals neuroinflammation with distinct microanatomical microglia-T-cell interactions. Immunity *54*, 1594-1610.e1511. 10.1016/j.immuni.2021.06.002.

48. Sefik, E., Qu, R., Junqueira, C., Kaffe, E., Mirza, H., Zhao, J., Brewer, J.R., Han, A., Steach, H.R., Israelow, B., et al. (2022). Inflammasome activation in infected macrophages drives COVID-19 pathology. Nature. 10.1038/s41586-022-04802-1.

49. Shimomura, Y., Agalliu, D., Vonica, A., Luria, V., Wajid, M., Baumer, A., Belli, S., Petukhova, L., Schinzel, A., Brivanlou, A.H., et al. (2010). APCDD1 is a novel Wnt inhibitor mutated in hereditary hypotrichosis simplex. Nature *464*, 1043-1047.

50. Stenman, J.M., Rajagopal, J., Carroll, T.J., Ishibashi, M., McMahon, J., and McMahon, A.P. (2008). Canonical Wnt signaling regulates organ-specific assembly and differentiation of CNS vasculature. Science *322*, 1247-1250.

51. Suda, Y., Nakashima, T., Matsumoto, H., Sato, D., Nagano, S., Mikata, H., Yoshida, S., Tanaka, K., Hamada, Y., Kuzumaki, N., and Narita, M. (2021). Normal aging induces PD-1-enriched exhausted microglia and A1-like reactive astrocytes in the hypothalamus. Biochem Biophys Res Commun *541*, 22-29. 10.1016/j.bbrc.2020.12.086.

52. Tai, L.M., Thomas, R., Marottoli, F.M., Koster, K.P., Kanekiyo, T., Morris, A.W., and Bu, G. (2016). The role of APOE in cerebrovascular dysfunction. Acta Neuropathol *131*, 709-723. 10.1007/s00401-016-1547-z.

53. Taquet, M., Luciano, S., Geddes, J.R., and Harrison, P.J. (2021). Bidirectional associations between COVID-19 and psychiatric disorder: retrospective cohort studies of 62 354 COVID-19 cases in the USA. Lancet Psychiatry *8*, 130-140. 10.1016/s2215-0366(20)30462-4.

54. Teuwen, L.-A., Geldhof, V., Pasut, A., and Carmeliet, P. (2020). COVID-19: the vasculature unleashed. Nature Reviews Immunology. 10.1038/s41577-020-0343-0.

55. Thakur, K.T., Miller, E.H., Glendinning, M.D., Al-Dalahmah, O., Banu, M.A., Boehme, A.K., Boubour, A.L., Bruce, S.S., Chong, A.M., Claassen, J., et al. (2021). COVID-19 neuropathology at Columbia University Irving Medical Center/New York Presbyterian Hospital. Brain. 10.1093/brain/awab148.

56. Thompson, A.J., Baranzini, S.E., Geurts, J., Hemmer, B., and Ciccarelli, O. (2018). Multiple sclerosis. Lancet *391*, 1622-1636. 10.1016/s0140-6736(18)30481-1.

57. Tran, K.A., Zhang, X., Predescu, D., Huang, X., Machado, R.F., Göthert, J.R., Malik, A.B., Valyi-Nagy, T., and Zhao, Y.Y. (2016). Endothelial β-Catenin Signaling Is Required for Maintaining Adult Blood-

Brain Barrier Integrity and Central Nervous System Homeostasis. Circulation *133*, 177-186. 10.1161/circulationaha.115.015982.

58. Visvabharathy, L., Hanson, B., Orban, Z., Lim, P.H., Palacio, N., Jain, R., Liotta, E.M., Penaloza-MacMaster, P., and Koralnik, I.J. (2021). Neuro-COVID long-haulers exhibit broad dysfunction in T cell memory generation and responses to vaccination. medRxiv. 10.1101/2021.08.08.21261763.

59. Wenzel, J., Lampe, J., Müller-Fielitz, H., Schuster, R., Zille, M., Müller, K., Krohn, M., Körbelin, J., Zhang, L., Özorhan, Ü., et al. (2021). The SARS-CoV-2 main protease M(pro) causes microvascular brain pathology by cleaving NEMO in brain endothelial cells. Nature neuroscience *24*, 1522-1533. 10.1038/s41593-021-00926-1.

60. Yang, A.C., Kern, F., Losada, P.M., Agam, M.R., Maat, C.A., Schmartz, G.P., Fehlmann, T., Stein, J.A., Schaum, N., Lee, D.P., et al. (2021). Dysregulation of brain and choroid plexus cell types in severe COVID-19. Nature *595*, 565-571. 10.1038/s41586-021-03710-0.

61. Yang, A.C., Stevens, M.Y., Chen, M.B., Lee, D.P., Stähli, D., Gate, D., Contrepois, K., Chen, W., Iram, T., Zhang, L., et al. (2020). Physiological blood-brain transport is impaired with age by a shift in transcytosis. Nature *583*, 425-430. 10.1038/s41586-020-2453-z.

62. Zhang, L., Zhou, L., Bao, L., Liu, J., Zhu, H., Lv, Q., Liu, R., Chen, W., Tong, W., Wei, Q., et al. (2021). SARS-CoV-2 crosses the blood-brain barrier accompanied with basement membrane disruption without tight junctions alteration. Signal Transduct Target Ther *6*, 337. 10.1038/s41392-021-00719-9.

63. Zhou, Y., Xu, J., Hou, Y., Leverenz, J.B., Kallianpur, A., Mehra, R., Liu, Y., Yu, H., Pieper, A.A., Jehi, L., and Cheng, F. (2021). Network medicine links SARS-CoV-2/COVID-19 infection to brain microvascular injury and neuroinflammation in dementia-like cognitive impairment. Alzheimers Res Ther *13*, 110. 10.1186/s13195-021-00850-3.

64. Zlokovic, B.V., Gottesman, R.F., Bernstein, K.E., Seshadri, S., McKee, A., Snyder, H., Greenberg, S.M., Yaffe, K., Schaffer, C.B., Yuan, C., et al. (2020). Vascular contributions to cognitive impairment and dementia (VCID): A report from the 2018 National Heart, Lung, and Blood Institute and National Institute of Neurological Disorders and Stroke Workshop. Alzheimer's & dementia : the journal of the Alzheimer's Association *16*, 1714-1733. 10.1002/alz.12157.

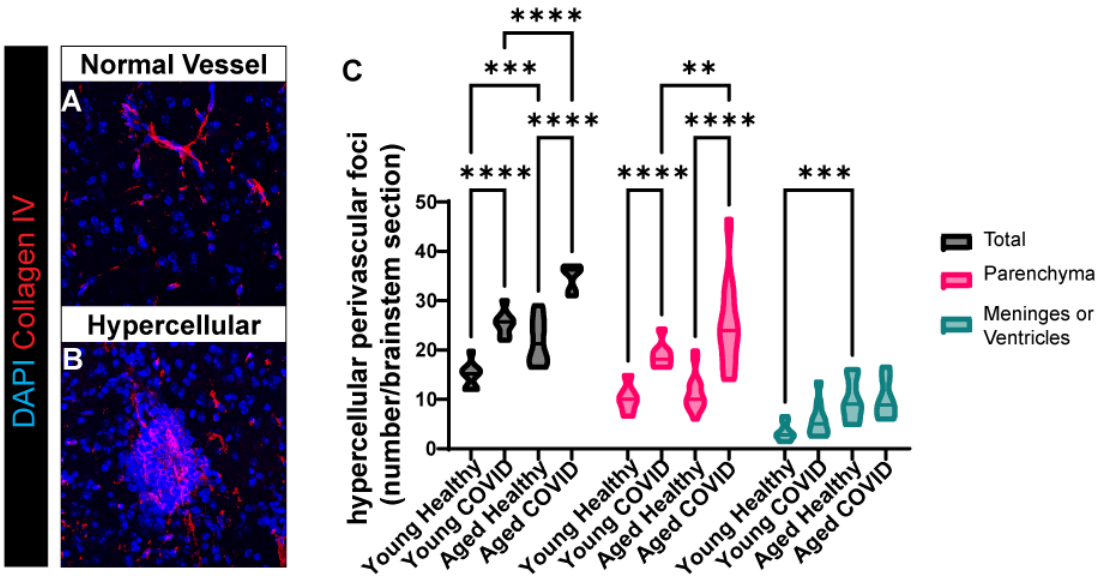
DAPI Collagen IV
Normal Vessel
A
Hypercellular
B
C
hypercellular perivascular foci (number/brainstem section)
Total
Parenchyma
Meninges or Ventricles
Young Healthy
Young COVID
Aged Healthy
Aged COVID

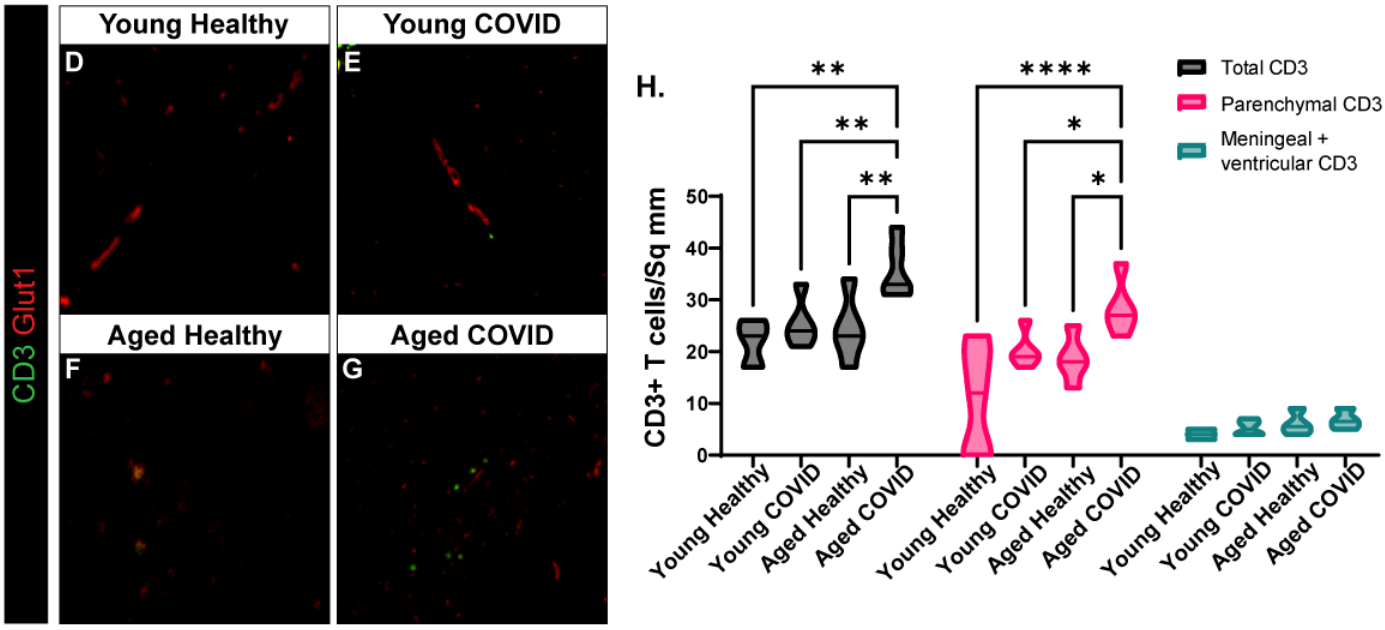
CD3 Glut1
Young Healthy
D
Young COVID
E
Aged Healthy
F
Aged COVID
G
H.
CD3+ T cells/Sq mm
Total CD3
Parenchymal CD3
Meningeal + ventricular CD3
Young Healthy
Young COVID
Aged Healthy
Aged COVID

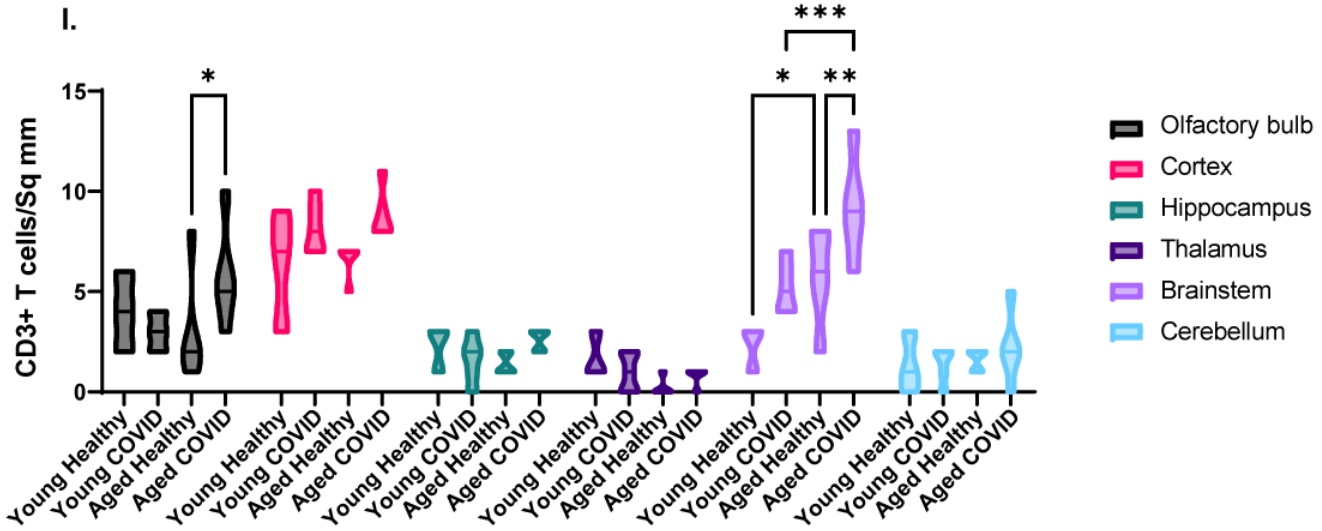
I.
CD3+ T cells/Sq mm
Olfactory bulb
Cortex
Hippocampus
Thalamus
Brainstem
Cerebellum
Young Healthy
Young COVID
Aged Healthy
Aged COVID

Figure 1. Age exacerbates cerebrovascular inflammation and T cell infiltration after respiratory SARS-CoV-2 infection. A-B) Immunofluorescent imaging of normal blood vessel (A) and a vessel with perivascular hypercellularity (B) characterized by DAPI (blue) nuclear cell counting and Collagen IV (red) to identify cerebrovascular basement membranes. C) Number of blood vessels with perivascular hypercellularity were manually counted in sagittal brain sections from young adult and middle-aged mice inoculated with SARS-CoV02 or vehicle. N= 9 mice 2-month-old vehicle, n=8 mice 2-month-old SARS-COV-2, n=9 mice 12-month-old vehicle, n=8 mice 12-month-old SARS-COV-2. Two-way ANOVA and Tukey's multiple comparisons test. D-G) T cell number and position were manually counted in sagittal brain sections immunostained with CD3 (green) and Glut1 (red). H) 12-month-old SARS-CoV-2 infected mice had significantly more CD3+ cells than 2-month-old SARS-CoV-2 infected mice. CD3+ cells touching parenchymal blood vessels and not touching ventricles or meninges were considered parenchymal. CD3+ T cells in the meninges or in the ventricles were considered meningeal/ventricular. I) CD3+ cell density in the indicated brain regions. Age exacerbated SARS-CoV-2 induced brain T cell infiltration. N=3 mice 2-month-old vehicle, n=5 mice 2-month-old SARS-COV-2, n=5 mice 12-month-old vehicle, n=5 mice 12-month-old SARS-COV-2. Two-way ANOVA and Tukey's multiple comparisons test.

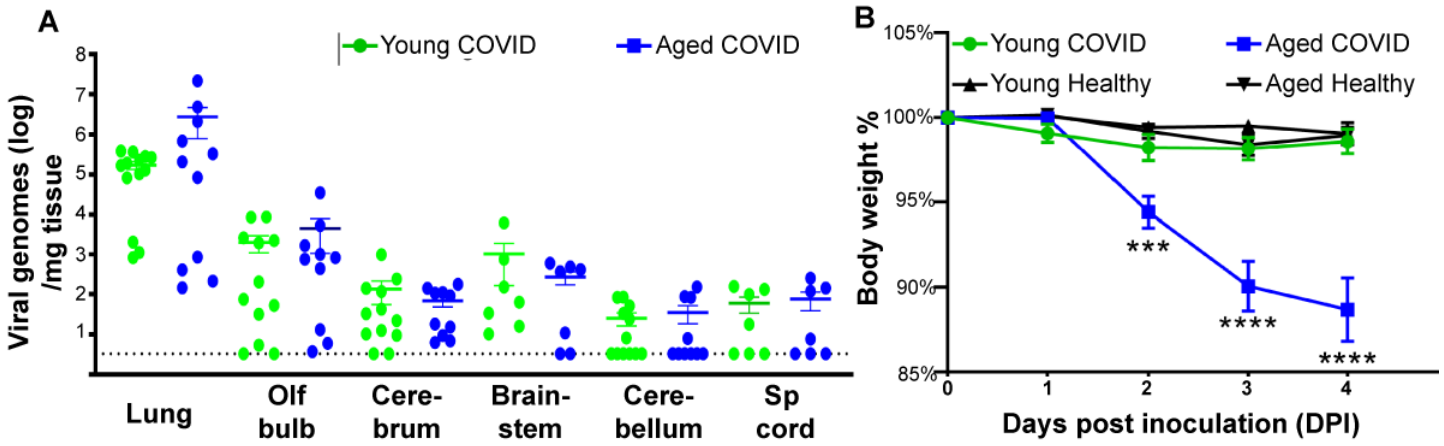

Figure 2. Viral RNA is present in similar amounts in brains of young and old C57Bl/6 mice after intranasal inoculation with SARS-CoV-2. A) Log scale scatterplot with median SARS-CoV-2 viral RNA detected by RT-PCR from the indicated tissues at 4 days post inoculation (DPI). No significant difference in SARS-CoV-2 viral genomes/tissue in young adult versus middle-aged adult. N=14 young SARS-COV-2, n=11 12-month-old SARS-COV-2, n=9 young vehicle, n=8 12-month-old vehicle. ANOVA and non-parametric Kruskal-Wallace multiple comparisons test. Dotted line indicates limit of detection. B) Body weight percent change in 2-month-old adult vehicle treated, 2-month-old SARS-COV-2 inoculated, 12-month-old adult vehicle treated, and 12-month-old adult SARS-COV-2 inoculated mice. $P<0.001$, $p<0.0001$, repeated-measures ANOVA with Sidak's multiple comparison test.

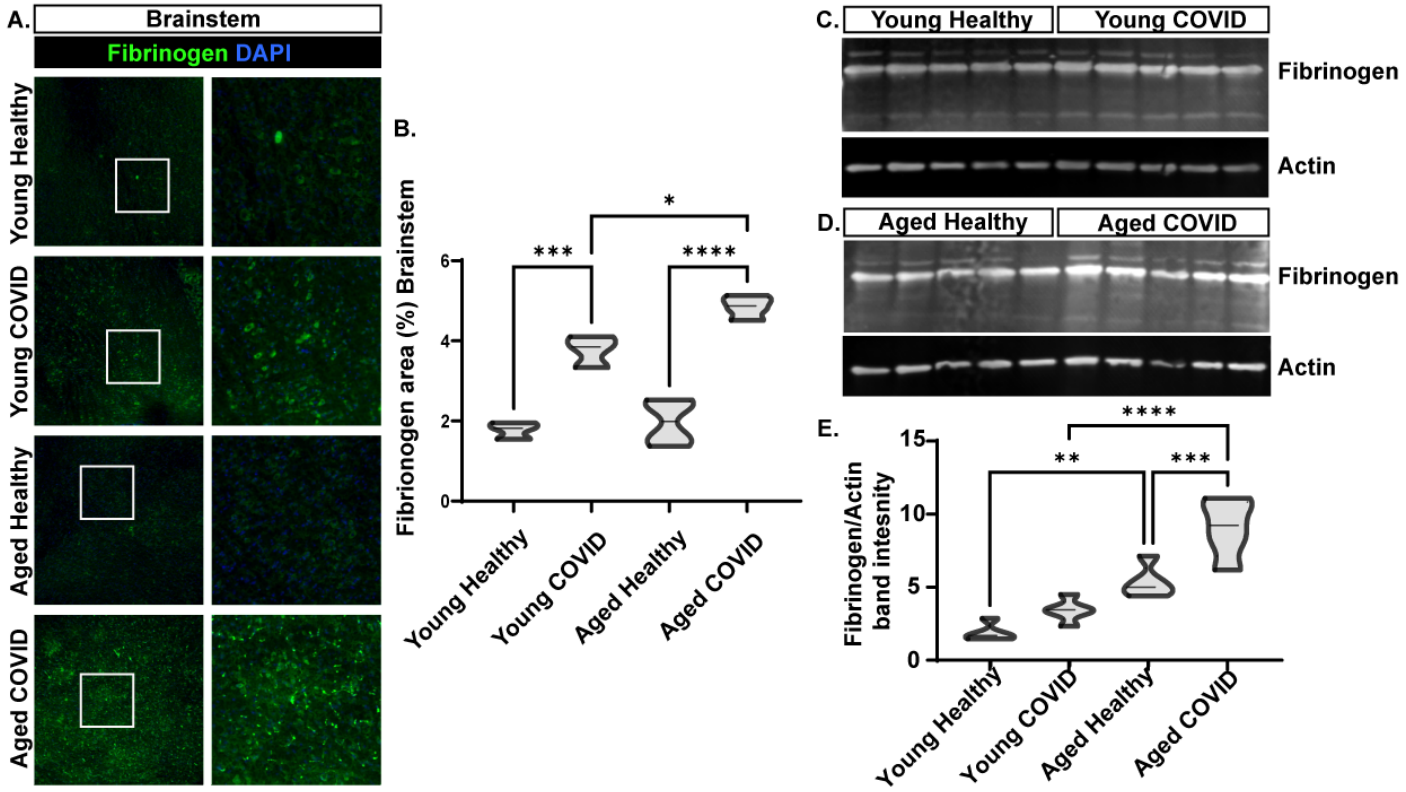

Figure 3. Age exacerbates blood-brain barrier leakage of fibrinogen in SARS-CoV-2 infected mice. A) Immunostaining for the inflammatory blood protein fibrinogen (green) in brainstem reticular formation of 2-month-old and 12-month-old mice 4 days after respiratory inoculation with SARS-CoV-2 or vehicle. B) Fibrinogen immunoreactivity was quantified in the brainstem reticular formation white matter of mice 4 days after SARS-COV-2 or vehicle inoculation. **p<0.01, ***p<0.001, ****p<0.0001, one way ANOVA and Sidak's multiple comparisons test. C-E) Western blot and quantification for fibrinogen (30kDa-70kDa bands) in brainstem homogenate obtained from 2-month-old (C) and 12-month-old mice (D) 4 days after inoculation with vehicle or SARS-CoV-2; n=5 per group. ***, p<0.01, one-way ANOVA and Sidak's multiple comparisons test.

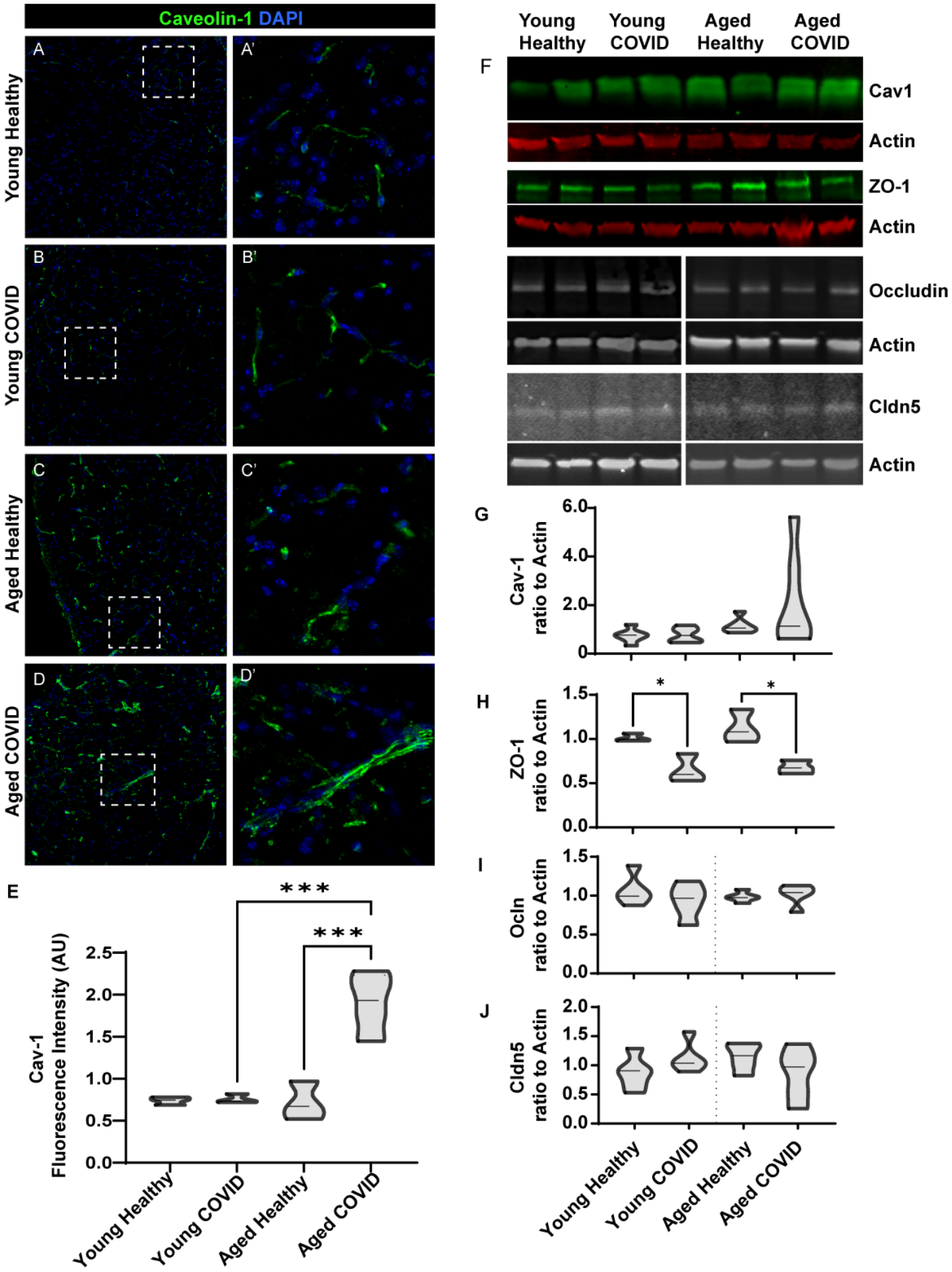
Caveolin-1 DAPI
A
A'
B
B'
C
C'
D
D'
Young Healthy
Young COVID
Aged Healthy
Aged COVID
E
Cav-1 Fluorescence Intensity (AU)
***
***
2.5
2.0
1.5
1.0
0.5
0.0
Young Healthy
Young COVID
Aged Healthy
Aged COVID
F
Young Healthy
Young COVID
Aged Healthy
Aged COVID
Cav1
Actin
ZO-1
Actin
Occludin
Actin
Cldn5
Actin
G
Cav-1 ratio to Actin
6.0
4.0
2.0
0
H
ZO-1 ratio to Actin
*
*
1.5
1.0
0.5
0.0
I
Ocln ratio to Actin
1.5
1.0
0.5
0.0
J
Cldn5 ratio to Actin
2.0
1.5
1.0
0.5
0.0
Young Healthy
Young COVID
Aged Healthy
Aged COVID

Figure 4. Age exacerbates upregulation of blood-brain barrier Caveolin-1 induced by SARS-CoV-2 inoculation. A-D) Immunostaining for Caveolin-1 (green) and DAPI nuclear stain (blue) in brainstem reticular formation of 2-month-old healthy, 2-month-old SARS-CoV-2, 12-month-old healthy, and 12-month-old SARS-CoV-2 infected mice at 4DPI. Higher magnification images of Caveolin-1 positive cerebrovasculature are shown in panels A', B', C', D'. E) Caveolin-1 mean fluorescence intensity in brainstem is significantly increased by age and infection. One-way ANOVA and Sidak's multiple comparisons test, n=3 per group. F) Western blot for transcellular and paracellular BBB proteins in brainstem homogenate from young and middle-aged mice inoculated with SARS-CoV-2 or vehicle. G) No significant differences in Caveolin-1 protein by Western blot. H) SARS-CoV-2 inoculation decreases brainstem ZO-1 protein quantity in all ages by Western blot, $p<0.05$. I-J) No significant differences in tight junction proteins Occludin and Claudin-5 by Western blot. Western blot data reflects n=5 mice per group, assessed by one-way ANOVA and Sidak's multiple comparisons test.

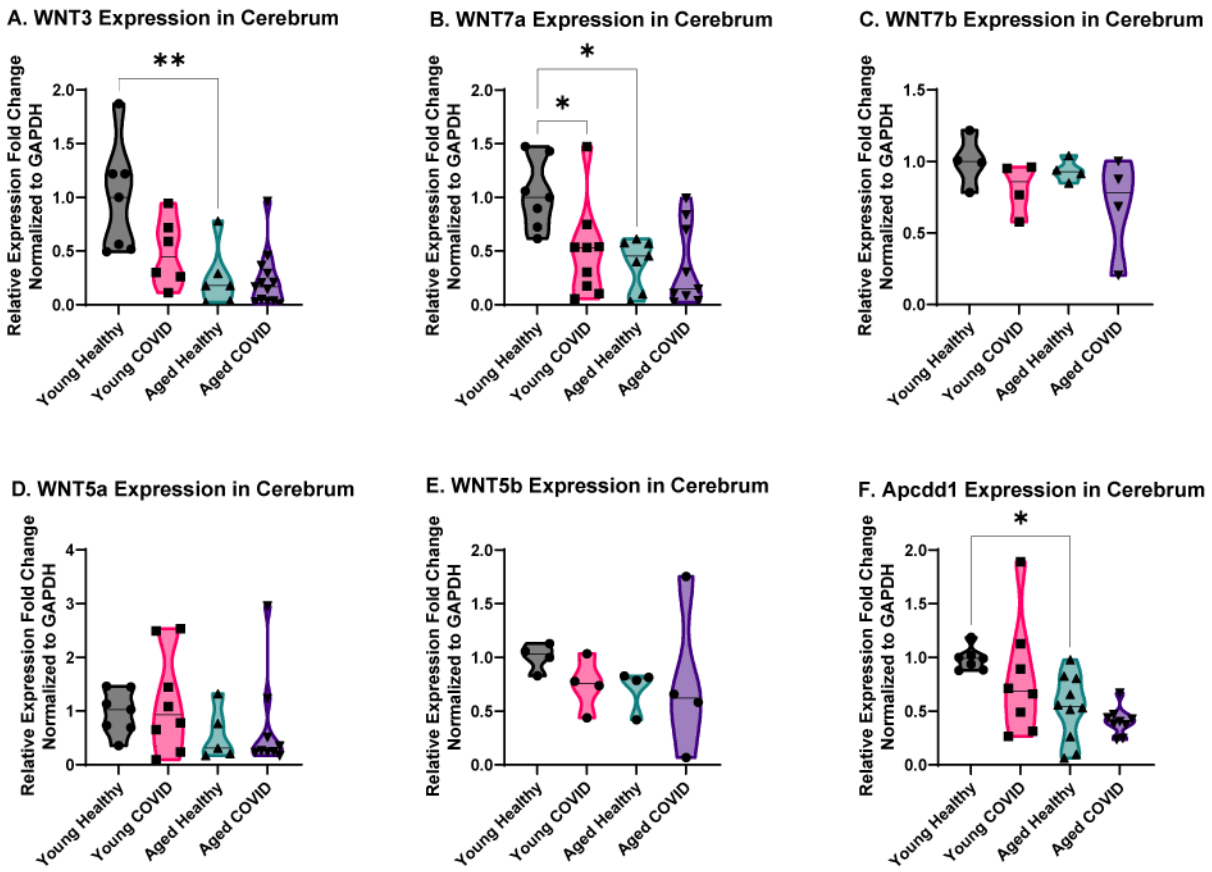

Figure 5. Canonical Wnt/β-catenin pathway components are decreased in the brain by aging and SARS-CoV-2 infection. Real-time quantitative PCR for Wnt ligands and Wnt/β-catenin transcriptional targets in brain homogenate of SARS-CoV-2 infected mice expressed as ΔΔCt values normalized to GAPDH. A) Canonical Wnt3 is decreased in normal aging. B-C) Canonical Wnt7a is decreased in aging and in SARS-CoV-2 infection. D-E) Non-canonical Wnt5a and Wnt5b are not significantly changed. F) Apcdd1, a β-catenin transcriptional target, is decreased in healthy aging. N=4 per group for Wnt3, Wnt7b, Wnt5b. N=7 per group for Wnt7a, Wnt5a, Apcdd1. *$p<0.05$, **$p<0.01$, one-way ANOVA and Sidak's multiple comparisons test.

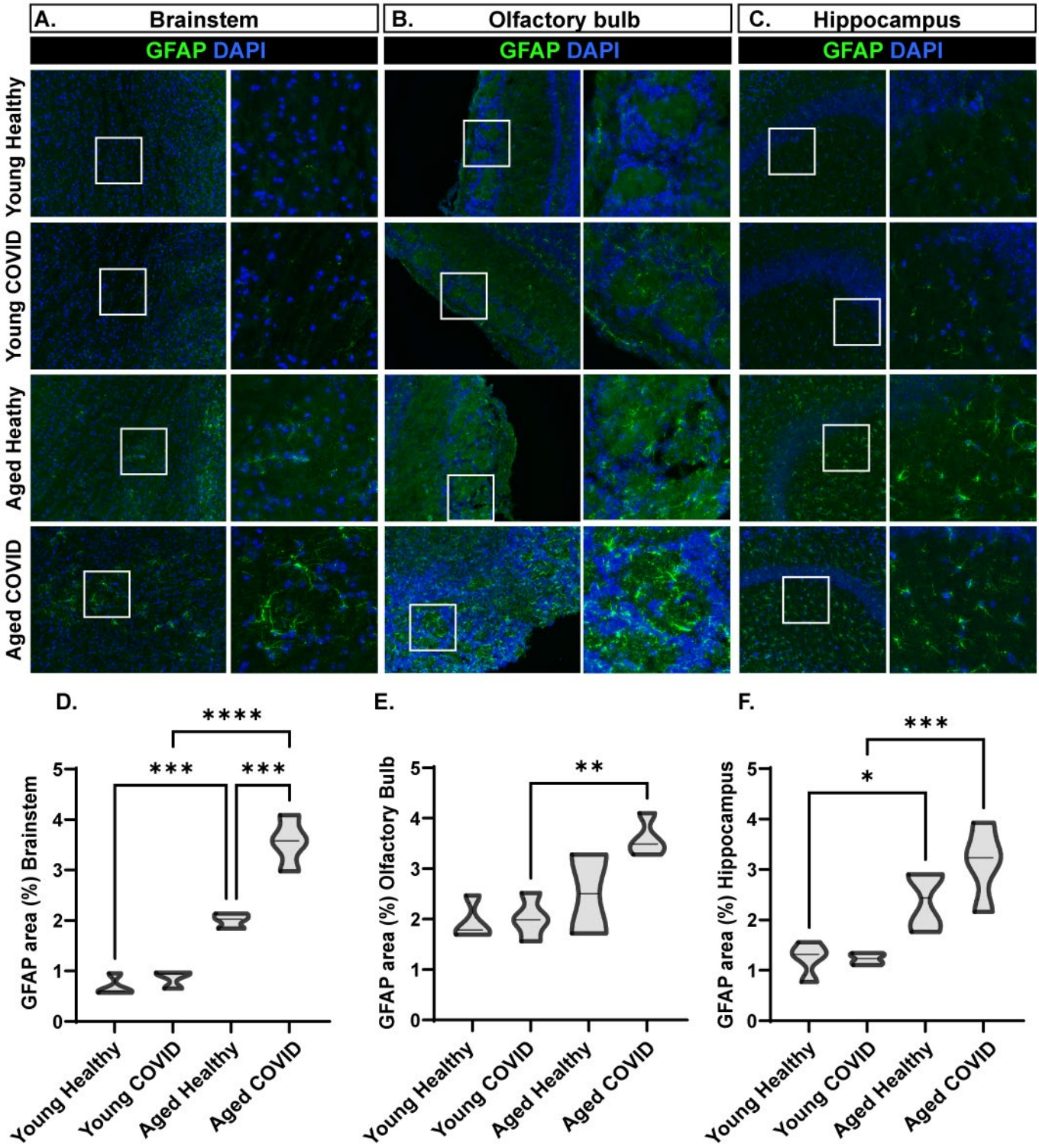

Figure 6. Age exacerbates astrocyte immunoreactivity for GFAP in mice inoculated with SARS-CoV-2. Percent area astrocyte immunoreactivity for GFAP (green) was identified by immunostaining in midline sagittal brain sections of 2-month-old and 12-month-old mice 4 days after inoculation with vehicle or SARS-CoV-2. A, D) Brainstem reticular formation white matter. B, E) Olfactory bulb. Quantification reflects olfactory glomerular layer only. C, F) Hippocampus. Quantification reflects CA1 stratum radiatum. Graphs shows averages of at

least three sections per mouse, n=3-4 mice per group. **p<0.01, ***, p<0.01, one-way ANOVA and Sidak's multiple comparisons test.

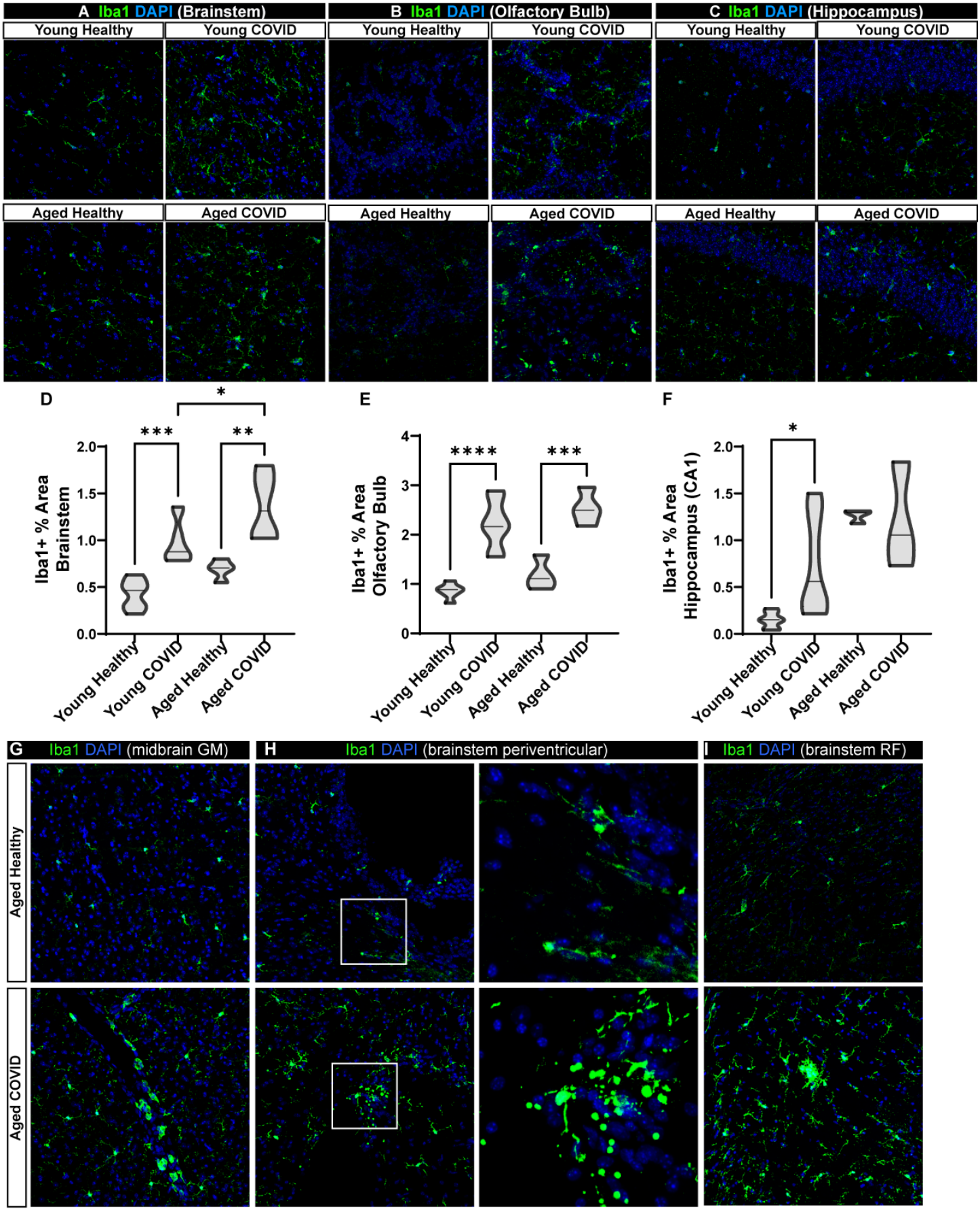

Figure 7. Microglial/monocyte Iba1 immunoreactivity is increased in brains of SARS-CoV-2 infected

mice. A-C) Representative confocal micrographs of microglia (Iba1+, green, DAPI, blue) in the brainstem reticular formation white matter (A), olfactory bulb glomerular layer (B), and hippocampal CA1 (C). D) Microglial (Iba1+) area quantification in the reticular formation of the brainstem of 2-month-old and 12-month-old mice 4 days after nasal inoculation with vehicle (saline) or SARS-CoV-2 MA-10. N=7 mice 2-month-old vehicle; n=9 mice 2-month-old SARS-COV-2; n=4 mice 12-month-old vehicle; n=4 mice 12-month-old SARS-COV-2. One-way ANOVA with Sidak's multiple comparison test, *$p<0.05$, **$p<0.01$, ***$p<0.001$. E) Microglial (Iba1+) area quantification in the olfactory bulb glomerular layer of 2-month-old and 12-month-old mice 4 days after nasal inoculation with vehicle (saline) or SARS-CoV-2 MA-10. N=7 mice 2-month-old vehicle; n=8 2-month-old SARS-COV-2; n=4 12-month-old vehicle; n=4 12-month-old SARS-COV-2. One-way ANOVA with Sidak's multiple comparison test, ***$p<0.001$, ****$p<0.0001$. F) Microglial (Iba1+) area quantification in the CA1 region of the hippocampus of 2-month-old and 12-month-old mice 4 days after nasal inoculation with vehicle (saline) or SARS-CoV-2 MA-10. N=7 2-month-old vehicle; n=9 2-month-old SARS-COV-2; n=3 12-month-old vehicle; n=3 per 12-month-old SARS-COV-2 mice. One-way ANOVA and Sidak's multiple comparisons test, *$p<0.05$. G) Microglia (Iba1+, green) near to a blood vessel in the gray matter have normal appearance in vehicle treated mice. A blood vessel in the gray matter of a young SARS-COV-2 mouse at 4DPI is invested with intense Iba1+ microglial processes and Iba1+ ameboid-shaped cells. H) Periaqueductal gray matter of the brainstem in 12-month-old infected mice contains numerous small round Iba1+ cells. I) Reticular white matter of the brainstem in 12-month-old infected mice contains increased microglial Iba1 reactivity and microglial nodules.

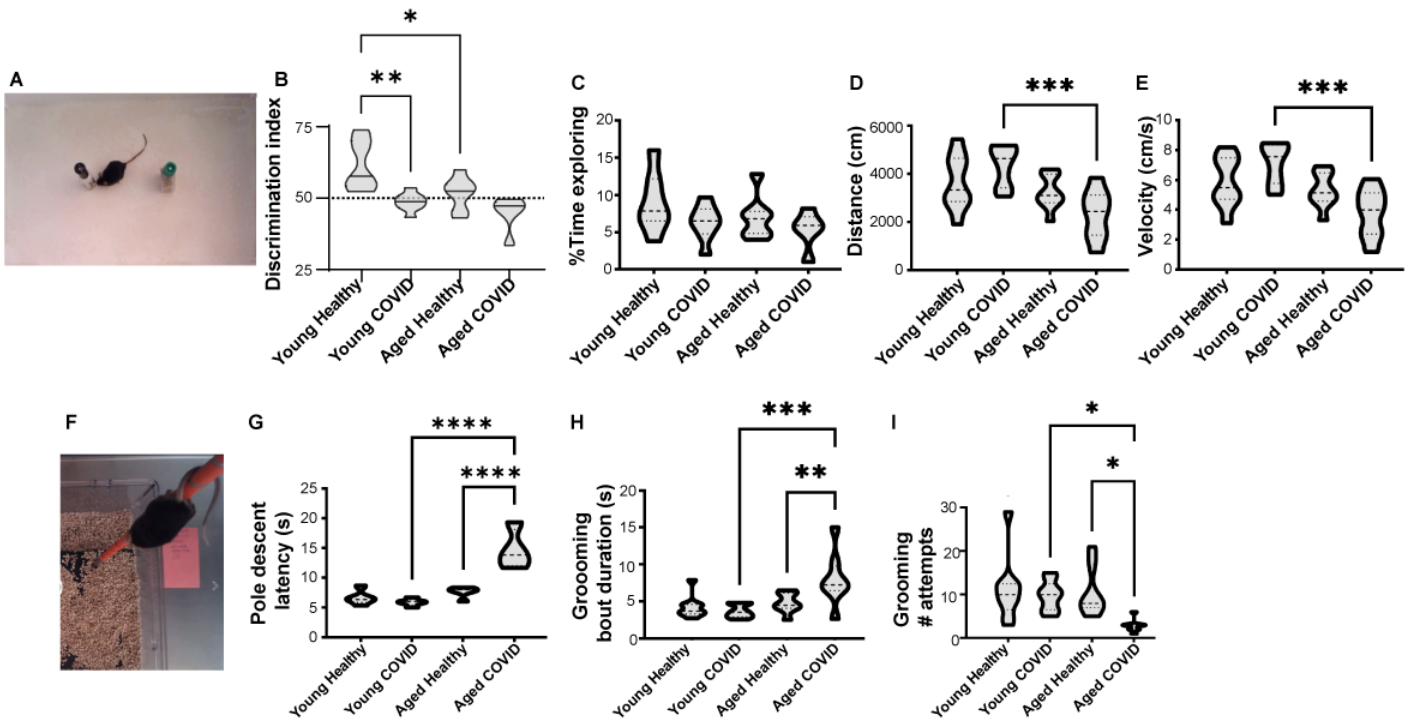

Figure 8. SARS-COV-2 respiratory infection causes neuropsychiatric abnormality in middle-aged but not young adult mice. A) Mouse with novel and familiar objects in open field behavior arena. B) Novel object recognition memory task. Young healthy mice preferentially attend to novel object (Discrimination Index >50% indicated by dotted horizontal line). Young mice infected with SARS-CoV-2, middle-aged healthy mice, and middle-aged mice infected with SARS-CoV-2 do not prefer the novel object. (n=5-8 per group) C) No significant differences in total exploration time between groups (n=5-8 per group). D) Decreased cumulative distance traveled by voluntary ambulation in the 12-month-old SARS-COV-2 mice (n=8-9 per group). E) Velocity of voluntary movement in the open field (n=8-9 per group). F-G) 12-month-old infected mice have significantly increased latency in the pole descent task, a complex motor coordination task involving brainstem/thalamic connectivity (n=5 per group). H) Duration of each bout of spontaneous grooming in the open field (n=8-9 per group). I) Number of spontaneous grooming bouts initiated in the open field (n=8-9 per group). *p<0.05, **p<0.01, ***p<0.001, ****p<0.0001, one-way ANOVA and Sidak's multiple comparisons test.